NAVAL POSTGRADUATE SCHOOL
Monterey, California

THESIS

MODELING THE COUPLED ROTOR/FUSELAGE RESPONSE OF THE H-3 SEA KING UTILIZING THE NPS FULL NONLINEAR RESPONSE

by

Salvatore P. Rafanello

March 1999

Co-Thesis Advisors:

E. Roberts Wood
Robert L. King

Approved for public release; distribution is unlimited.

19990415015

REPORT DOCUMENTATION PAGE

Form Approved
OMB No. 0704-0188

1. AGENCY USE ONLY *(Leave blank)*	2. REPORT DATE March 1999	3. REPORT TYPE AND DATES COVERED Master's Thesis	
4. TITLE AND SUBTITLE MODELING THE COUPLED ROTOR/FUSELAGE RESPONSE OF THE H-3 SEA KING UTILIZING THE NPS FULL NONLINEAR RESPONSE			**5. FUNDING NUMBERS**
6. AUTHOR(S) Rafanello, Salvatore P.			
7. PERFORMING ORGANIZATION NAME(S) AND ADDRESS(ES) Naval Postgraduate School Monterey, CA 93943-5000			**8. PERFORMING ORGANIZATION REPORT NUMBER**
9. SPONSORING / MONITORING AGENCY NAME(S) AND ADDRESS(ES)			**10. SPONSORING/MONITORING AGENCY REPORT NUMBER**

11. SUPPLEMENTARY NOTES
The views expressed in this thesis are those of the author and do not reflect the official policy or position of the Department of Defense or the U.S. Government.

12a. DISTRIBUTION / AVAILABILITY STATEMENT Approved for public release; distribution is unlimited.	12b. DISTRIBUTION CODE

13. ABSTRACT *(Maximum 200 words)*

Adapting the Naval Postgraduate School full nonlinear simulation model of coupled rotor/fuselage response to the H-3 Sea King, the concentration of this work rests on validating the rotor simulation against an actual rotorcraft. The parameters of the H-3 from the characteristic equation of a modeled mass-spring-damper system are inputted into a five-bladed model initially utilizing MAPLE to process LaGrange's equation defining the helicopter's full set of nonlinear equations of motion. Results are converted to MATLAB and are then processed in SIMULINK returning time history plots of blade/fuselage motion. Conclusions are in accordance with literature of Coleman, Feingold and Deutsch.

14. SUBJECT TERMS Helicopter ground resonance, mechanical instability, dynamics, MAPLE, MATLAB, SIMULINK, Hilbert transform			15. NUMBER OF PAGES 93
			16. PRICE CODE

17. SECURITY CLASSIFICATION OF REPORT Unclassified	18. SECURITY CLASSIFICATION OF THIS PAGE Unclassified	19. SECURITY CLASSIFICATION OF ABSTRACT Unclassified	20. LIMITATION OF ABSTRACT UL

MODELING THE COUPLED ROTOR/FUSELAGE RESPONSE OF THE H-3 SEA KING UTILIZING THE NPS FULL NONLINEAR RESPONSE

Salvatore P. Rafanello
Lieutenant , United States Navy
B.S., United States Naval Academy, 1990
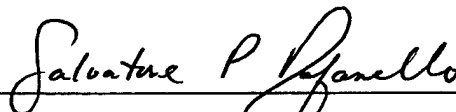
Submitted in partial fulfillment of the
requirements for the degree of

MASTER OF SCIENCE IN AERONAUTICAL ENGINEERING

from the

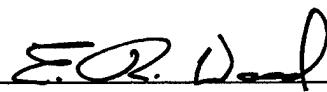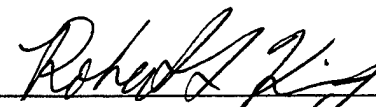## NAVAL POSTGRADUATE SCHOOL
March 1999
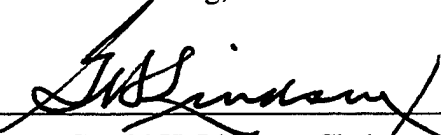
Author: _____
Salvatore P. Rafanello

Approved by: _____
E. Roberts Wood, Co-Thesis Advisor

_____
Robert L. King, Co-Thesis Advisor

_____
Gerald H. Lindsey, Chairman
Department of Aeronautics and Astronautics

iii

ABSTRACT

Adapting the Naval Postgraduate School full nonlinear simulation model of coupled rotor/fuselage response to the H-3 Sea King, the concentration of this work rests on validating the rotor simulation against an actual rotorcraft. The parameters of the H-3 from the characteristic equation of a modeled mass-spring-damper system are inputted into a five-bladed model initially utilizing MAPLE to process LaGrange's equation defining the helicopter's full set of nonlinear equations of motion. Results are converted to MATLAB and are then processed in SIMULINK returning time history plots of blade/fuselage motion. Conclusions are in accordance with literature of Coleman, Feingold and Deutsch.

TABLE OF CONTENTS

LIST OF FIGURES

LIST OF TABLES

ACKNOWLEDGEMENT

I would like to personally thank both of my thesis advisors for their continued support throughout my entire thesis research. From the beginning to the end, their "open door policy" made this unique learning opportunity not only a rewarding experience, but enjoyable as well.

I. INTRODUCTION

A. DISCUSSION

The helicopter is a complex system operating in several degrees of freedom. Should negative damping be present in the system, dynamic coupling between the rigid body motion of the fuselage and oscillations of the rotor blades in their plane of rotation can result in the self-excited vibration known as ground resonance. If not counteracted, this destructive phenomenon will destroy the aircraft in seconds.

The sequence of events leading into the mechanical instability can be started if the helicopter is subjected to a hard one wheel landing, taxiing over an uneven surface, or any number of initial rates and/or displacements in primarily the roll and lateral movement of the hub. Blades are then placed out of pattern resulting in an unbalance of the centrifugal forces at the head. The aircraft now begins to roll more on its landing gear allowing further increases in the rates and displacements of the hub. This violent cycle, if uncorrected, will lead to increasing oscillatory amplitude of the helicopter about its landing gear until the ship tips over or breaks up.

The corrective measure to suspected ground resonance is to immediately become airborne. This procedure alters the rigid body natural frequencies of the aircraft thereby changing the coupled modes between the fuselage and the rotor head. Once airborne, the helicopter oscillations dampen out as a result of lower roll and lateral natural frequencies.

As power is brought on, the helicopter becomes "light on the skids". A rotorcraft's natural frequency depends upon its percent airborne condition primarily in part because the oleo has an air spring where the spring rate is dependent upon the deflection. Therefore, a stationary helicopter transitioning to hover may become susceptible to ground resonance as its natural frequency is changed while becoming partially airborne.

Today, engineers design helicopters to avoid ground resonance by altering the parameters of the systems that govern the natural frequency and damping of the aircraft. The primary parameters available to the design engineer include blade damping, oleo damping, oleo spring rate, tire spring rate and landing gear tread width. Beside general

1

knowledge of a helicopter's susceptibility to ground resonance, pilots as well as maintenance personnel should be familiar with their aircraft's potential reaction to blown dampers and improperly serviced landing gear struts.

B.   BACKGROUND

Remarkably, the 1940's gave birth to the study of ground resonance. Robert Coleman, the forefather in the field of helicopter mechanical instability was the first to address the problem of ground resonance [Ref. 1] and [Ref. 2]. He found the primary modes likely to be excited in the normal operation of the rotorcraft were the hinged deflection of the blades in their plane of rotation and rigid body fuselage modes contributing to horizontal deflection of the pylon. This meant the landing gear deflections that produced lateral motion at the top of the pylon were extremely important. Soon after, M. L. Deutsch consolidated the results of Coleman by developing a quantitative analysis of the damping required to keep the helicopter free of resonant modes [Ref. 3]. Both analyses were before their time and required the arrival of computerized techniques to more accurately evaluate ground and air resonance.

At the Naval Postgraduate School (NPS), a full nonlinear simulation model of coupled rotor /fuselage interaction was created by LT Christopher S. Robinson in March of 1997, [Ref. 4]. The NPS modeler is an analysis tool that initially utilizes MAPLE to process LaGrange's equation defining the helicopter full set of nonlinear equations of motion. The equations of motion that result are returned as either FORTRAN or C and can be readily converted to the MATLAB programming language. The converted MATLAB result is incorporated into a SIMULINK S-function, producing time history plots of blade/fuselage motion. The fundamental difference between the NPS modeler and other dynamic modelers, such as the University of Maryland's UMARC, is the development of the complete set of nonlinear terms in the equations of motions. Formulated in full nonlinear form, there are no ordering schemes, no small angle assumptions, and no linearizing techniques or simplifying assumptions used in the development of the equations of motion utilized by the NPS modeler.

2

The generic model presented in Robinson's thesis demonstrated a hypothetical aircraft's reaction to ground resonance. Building upon his three-bladed model, Robert King, a thesis co-advisor, developed a five-bladed model that required evaluation. Utilizing the data prepared by E. Roberts Wood, a thesis co-advisor, [Ref. 5], the H-3 Sea King helicopter was adapted to the NPS ground resonance modeler.[1] A mass-spring-damper system of the H-3's landing gear was examined to obtain the parameters to enter into the NPS simulation. A thorough analysis of the natural frequencies (ω_p) in the lateral and roll modes at three power settings of 0/20/80 percent airborne were made with respect to the literature prepared by Coleman, Feingold and Deutsch. Stability charts were developed from the tailored data of the Sea King and compared with the modeler's results.

Previously, the lack of a design tool that could predict both the linear and non-linear portion of the stability characteristic curves required expensive and time consuming wind tunnel tests to confirm rotor/fuselage stability. Beside verification of the NPS modeler to a well-known rotorcraft, continued development of this project may someday assist engineers in developing new airframes well clear of all ground resonance regimes. Further, amplifying information to Coleman, Feingold and Deutsch is presented for all Naval Postgraduate School students as well as others who wish to expand their knowledge in this field of study.

---

[1] Wood's report "Preliminary Report on Mechanical Instability of HSS-2 Helicopters" was prepared while at Sikorsky in 1958. The H-3 is a descendant of the HSS-2.

II.   MASS-SPRING-DAMPER MODEL

A.   WOOD'S MODEL

A helicopter is a complex structure that can be modeled as a mass-spring-damper system in several degrees of freedom. The landing gear structure is modeled as a spring-damper system by considering the spring rates in the tires, oleos and structural supports. Wood's system depicted below in Figure (1) was used to model the H-3 [Ref. 5]. It is a modified 2-DOF system specifically designed to assess the roll and lateral modes of the helicopter since they typically couple with the regressive lag frequency of the hub progressing into ground resonance.
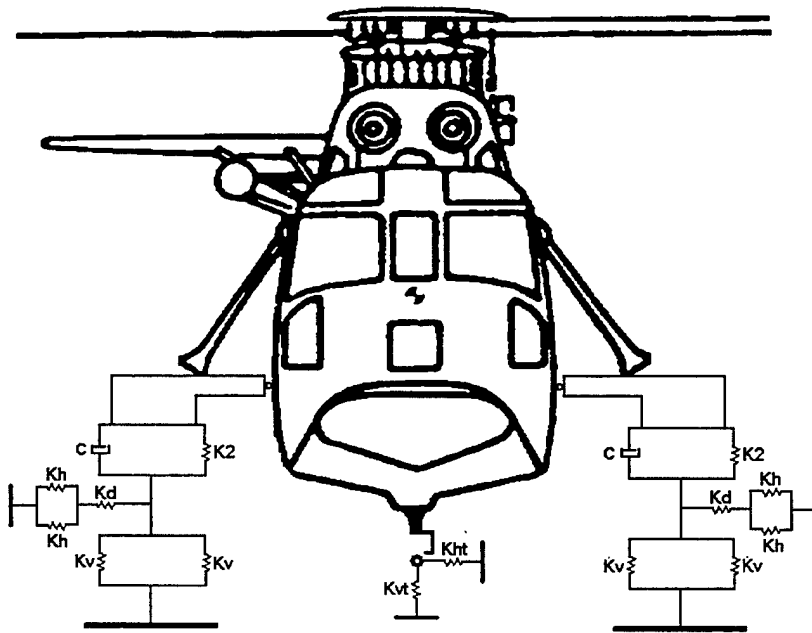
$K_h \equiv$ main landing gear tire lateral spring rate
$K_v \equiv$ main landing gear vertical tire spring rate
$K_d \equiv$ main landing gear structural lateral spring rate
$K_2 \equiv$ main landing gear oleo spring rate
$K_{ht} \equiv$ tail landing gear lateral spring rate
$K_{vt} \equiv$ tail landing gear vertical spring rate
C $\equiv$ main landing gear oleo damping

Figure 1. H-3 Mass-Spring-Damper System

Table (1) is a list corresponding to the spring rates of the tires, oleos and landing gear structural support depicted above in Figure (1).

	Spring Rate (lbs/in)		
	0% Airborne	20% Airborne	80% Airborne
K_h	807	850	975
K_v	1925	1875	1300
K_d	18,500	18000	8000
K_2	2967	1860	116
K_{ht}	743	766	877
K_{vt}	1500	1475	1050
C (lb-sec/in)	30	30	30

Table 1. H-3 Model Parameters

Combining the spring and dampers in Figure (1) to simplify the system and then equating the appropriate horizontal and vertical reactions with their respective deflections, Wood solves for the roll spring rate and the roll damping from the complex value of the resisting moment of the aircraft through the angle Θ.

$$M = M_r + jM_I$$

$$K_\Theta = \frac{M_r}{\Theta}$$

$$C_\Theta = \frac{M_I}{W}$$

where $W \equiv$ ground resonance exciting frequency or $\Omega \pm W\phi'$

6

The modified system along with the simplified values are depicted below in Figure (2) and Table (2). The reader is encouraged to reference Wood's derivation for amplification.
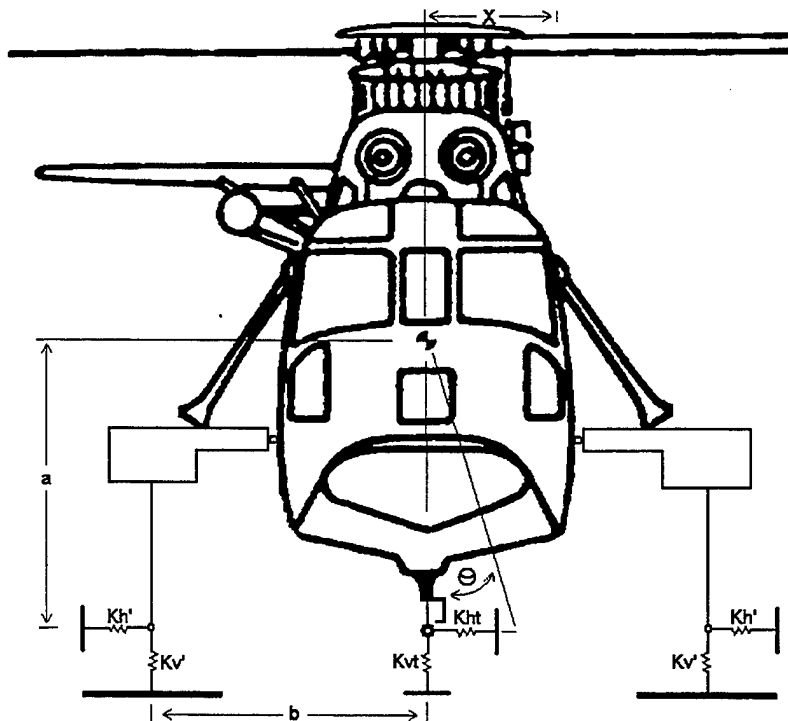
$K_{h'}$ ≡ combination of main landing gear tire lateral spring rates
$K_{v'}$ ≡ combination of main landing gear tire vertical spring rates
K_{hhat} ≡ combination of main and tail landing gear lateral spring rates
K_θ ≡ real part of complex value of resisting moment rolled through angle Θ

Figure 2. Modified H-3 Mass-Spring-Damper System

| | Spring Rate (lbs/in) | | |
	0% Airborne	20%Airborne	80% Airborne
$K_{h'}$	1485	1553	1568
$K_{v'}$	3850	3750	2600
K_{hhat}	3712	3873	4013
K_θ (in-lbs/rad)	3.91E+07	3.50E+07	2.80E+07

Table 2. Consolidated Spring Rates

7

The derivation of the coupled frequency equation of the H-3 model in Figure (2) is presented and also simplified by Wood [Ref.5].

$$M\ddot{x} + (2K_{H'} + K_{HT})x + (2K_{H'} + K_{HT})a\Theta = 0$$
$$I\ddot{\Theta} + (2K_{H'} + K_{HT})ax + 2K_V b^2\Theta + (2K_{H'} + K_{HT})a^2\Theta = 0$$

allowing,

$$2K_{H'} + K_{HT} = \overline{K}_H$$
$$M\ddot{x} + \overline{K}_H x + \overline{K}_H a\Theta = 0$$
$$I\ddot{\Theta} + K_\Theta \Theta + \overline{K}_H ax = 0$$

assuming harmonic motion where,

$$X = A\sin(\omega_p t + \phi_1) \quad \text{and} \quad \theta = B\sin(\omega_p t + \phi_2)$$
$$\text{yields,}$$
$$(-M\omega_p^2 + \overline{K}_H)A + (\overline{K}_H a)B = 0$$
$$(\overline{K}_H a)A + (-I\omega_p^2 + K_\Theta)B = 0$$

The tabulated data in Table (1) and Table (2) is then entered into a MATLAB program called COUPLEDFREQ.m located in Appendix A. Besides confirming all the spring rate values in Wood's report, COUPLEDFREQ.m also calculates the natural frequencies (ω_p) for both the lateral and roll modes of the H-3 at three different power configurations by solving the eigenvalue/eigenvector problem.

Where,

$$Ax = \lambda x$$
$$(\frac{\overline{K}_H}{M})A + (\frac{\overline{K}_H a}{M})B = w_p^2 A$$
$$(\overline{K}_H a)A + (\frac{K_\Theta}{I})B = w_p^2 B$$

$$\begin{vmatrix} A_{11} & A_{12} \\ A_{21} & A_{22} \end{vmatrix} \begin{vmatrix} A & A \\ B & B \end{vmatrix} = \begin{vmatrix} \lambda_1 & 0 \\ 0 & \lambda_2 \end{vmatrix} \begin{vmatrix} A & A \\ B & B \end{vmatrix}$$ where $\lambda_1, \lambda_2 \equiv w_p^2$ in lateral and roll mode respectively

$$A_{11}A + A_{12}B = \lambda_1 A$$

$$A_{21}A + A_{22}B = \lambda_2 B$$

$$\begin{vmatrix} \dfrac{\overline{K}_H}{M} & \dfrac{\overline{K}_H}{M}a \\ \dfrac{\overline{K}_H}{I}a & \dfrac{K_\Theta}{I} \end{vmatrix} \begin{vmatrix} A & A \\ B & B \end{vmatrix} = \begin{vmatrix} \lambda_1 & 0 \\ 0 & \lambda_2 \end{vmatrix} \begin{vmatrix} A & A \\ B & B \end{vmatrix}$$

The natural frequencies for both the roll and lateral modes at their corresponding power settings are shown below in Table (3).

	0% Airborne		20% Airborne		80% Airborne	
Mode	rad/sec	cycle/min	rad/sec	cycle/min	rad/sec	cycle/min
roll	17.78	169.79	17.30	165.20	16.79	160.33
lateral	6.25	59.68	5.67	54.14	2.18	20.82

Table 3. Natural Frequencies of Roll and Lateral Modes

B. VIRTUAL POINT OF ROTATION

The ratio B/A obtained from the eigenvector is equivalent to Θ/X without any phase shift considered in the evaluation. More specifically, the ratio of the roll displacement in radians to the lateral displacement in inches is known. With this ratio, normalized power charts based upon one inch of lateral movement, represented by the horizontal line, are then generated depicting the virtual point of rotation for the roll and lateral modes individually.

1. Roll Mode

Evaluating the roll mode first in Figure (3), the primary result is that the point of rotation is above the center of gravity of the H-3 for all three power settings. As power is brought on the aircraft, the point of rotation will continue to increase along the vertical

9

axis of the helicopter. In fact, Prouty [Ref. 6] mentions that once the helicopter breaks the ground, the point of rotation can be estimated at seven rotor lengths above the helicopter.

Virtual Point of Rotation (Roll)-0% PWR Airborne

Virtual Point of Rotation (Roll)-80%PWR Airborne
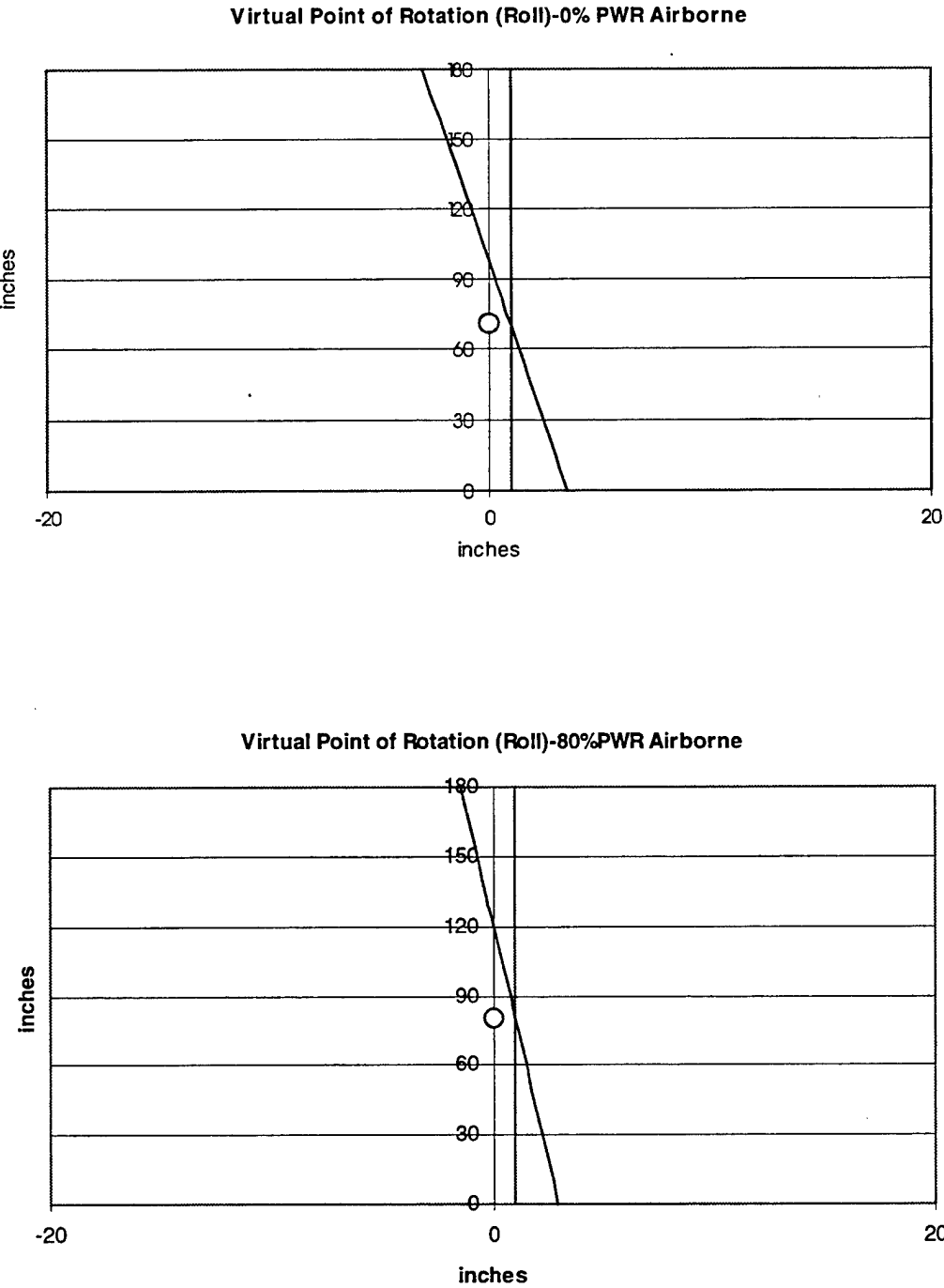
Figure 3. Virtual Point of Rotation-Roll Mode 0% and 80% PWR Airborne

Below in Figure (4), the H-3 is superimposed over the line of rotation for the 20%
power case. In this scenario, as the aircraft is displaced 10 inches in the lateral direction,
its roll angle will be 18.04°. Incidentally, this is greater than the 15° dynamic tipover
angle of the H-3.
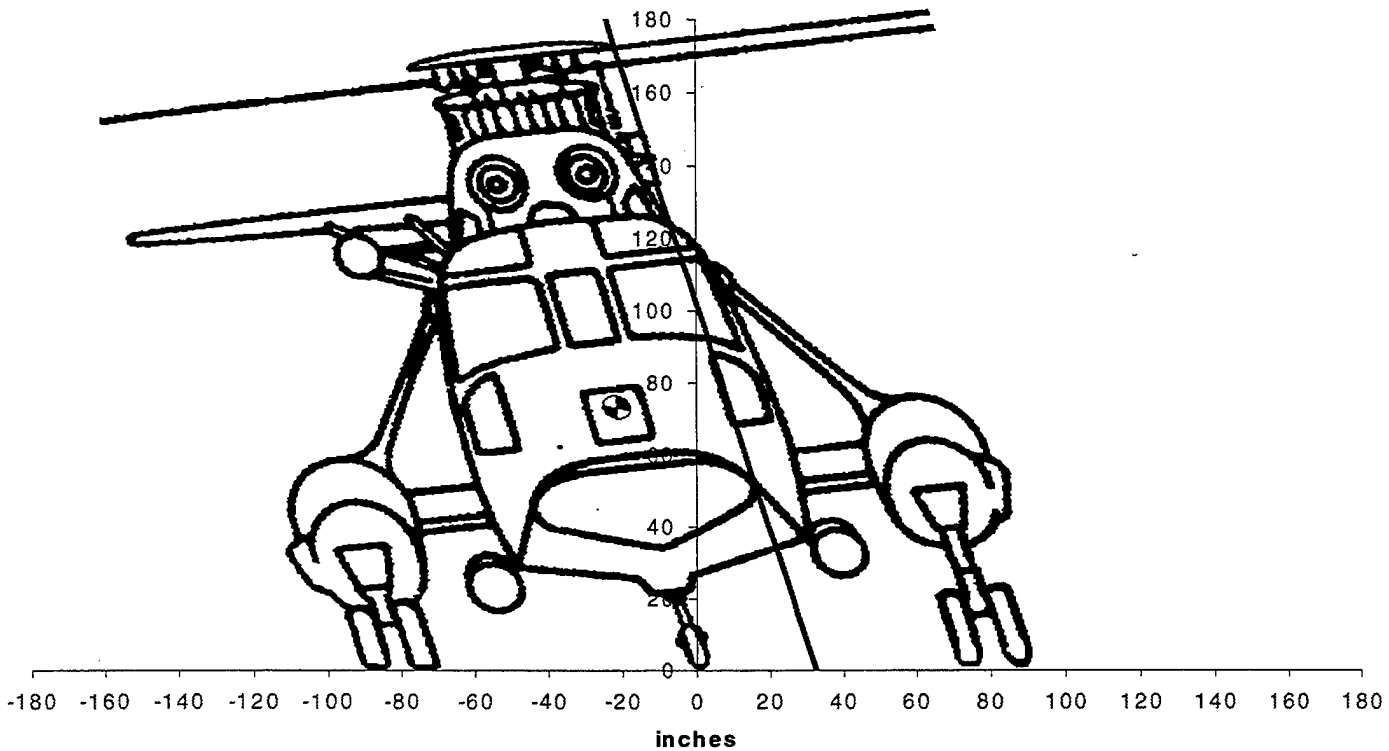
Figure 4. Virtual Point of Rotation-Roll Mode 20% PWR Airborne

2. Lateral Mode

Conversely, the lateral mode has its virtual point of rotation underground. As
power is applied to the H-3, similar to the roll mode and in accordance with Prouty [Ref.
6], the point of rotation begins to increase along the vertical line of the aircraft.

11

Virtual Point of Rotation (Lateral) -0% PWR Airborne
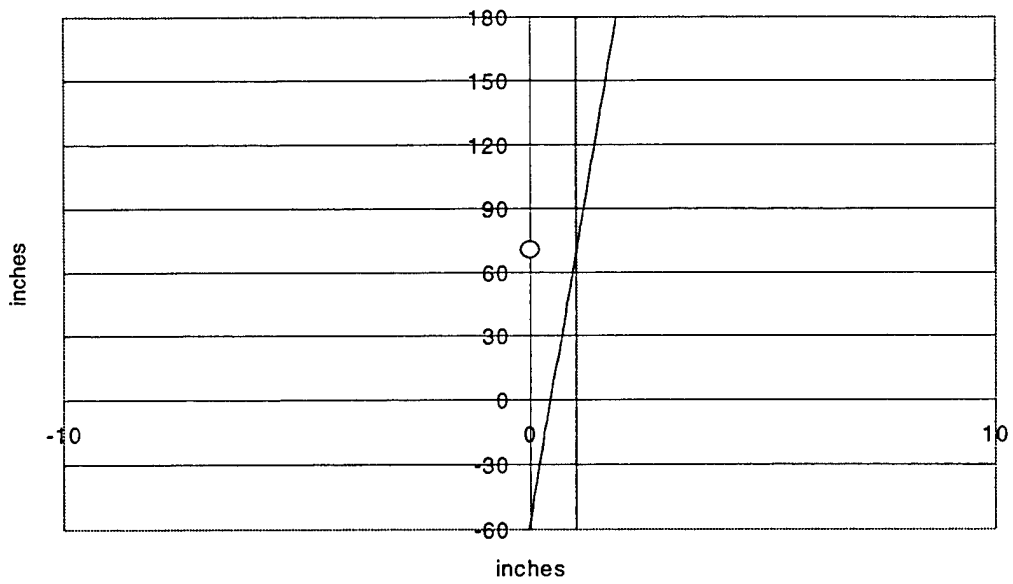
Virtual Point of Rotation (Lateral)-80% PWR Airborne
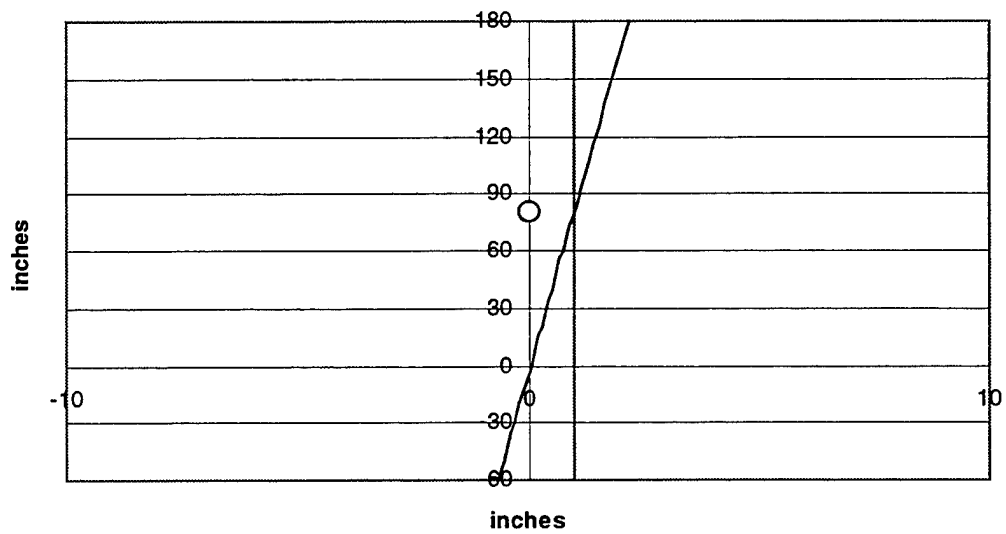
Figure 5. Virtual Point of Rotation-Lateral Mode 0% and 80% PWR Airborne

12

For comparison and ease of understanding, the H-3 is once again superimposed over the line of rotation in Figure (6) for the 20% power case. In the lateral mode, 10 inches of displacement in the X direction is equivalent to –5.21° of roll.
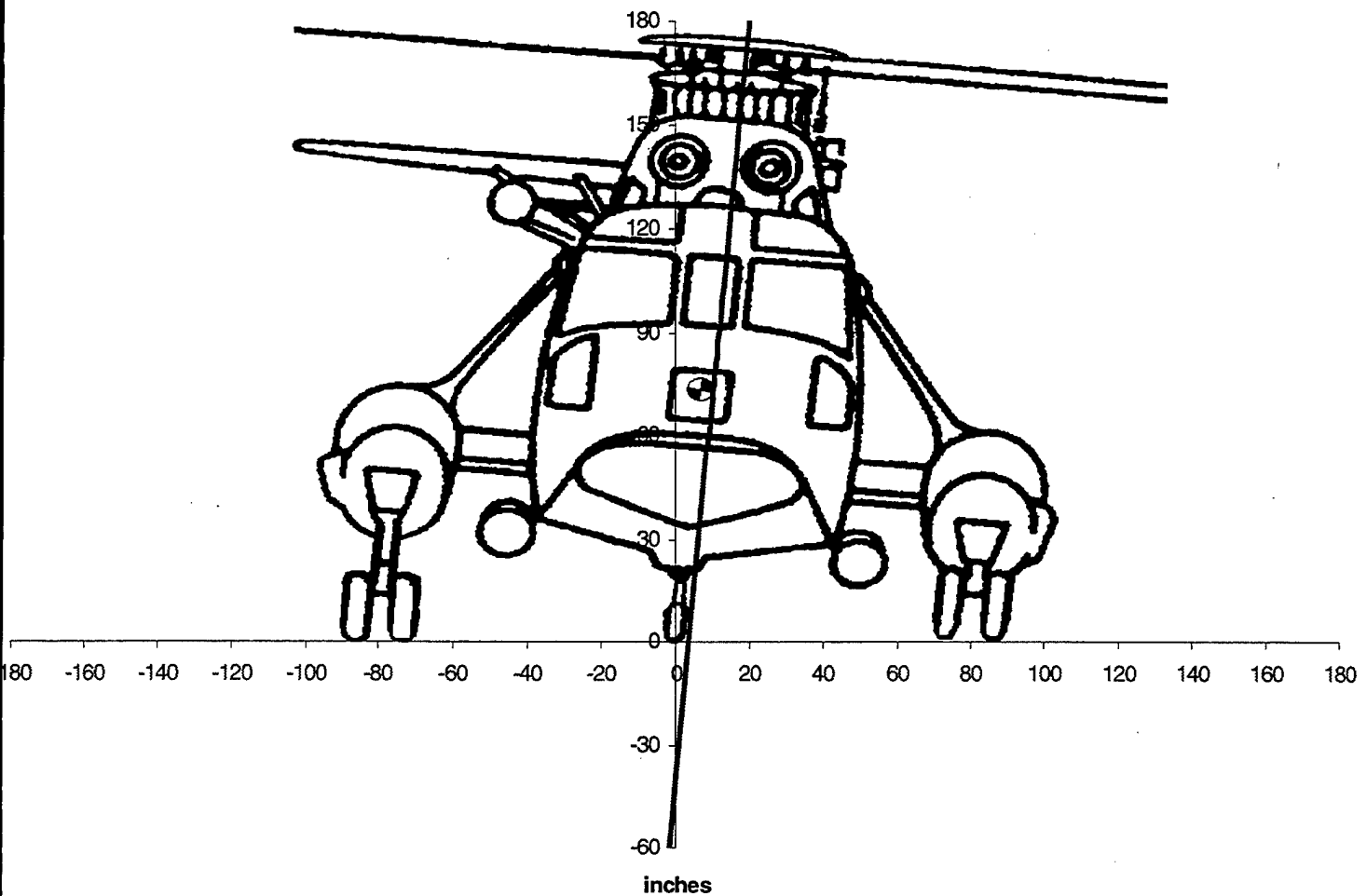
Figure 6. Virtual Point of Rotation-Lateral Mode 20% PWR Airborne

III.   NPS GROUND RESONANCE MODELER

A.   DISCUSSION OF MODELER

The NPS full nonlinear simulation of coupled rotor /fuselage interaction is a dedicated Coleman analysis tool that initially utilizes MAPLE to process LaGrange's equation defining the helicopter full set of nonlinear equations of motion.[2]

$$\frac{d}{dt}\left(\frac{\partial T}{\partial \dot{q}_i}\right) - \frac{\partial T}{\partial q_i} + \frac{\partial U}{\partial q_i} + \frac{\partial D}{\partial \dot{q}_i} = F_i$$

where T is kinetic energy, U potential energy, D the dissipation function, F_i a generalized force and q_i is a generalized displacement.

The results are returned as either FORTRAN or C and can be readily converted to MATLAB. From this point, the MATLAB results are processed in SIMULINK resulting in time history plots of blade/fuselage motion. Expanding upon the work previously performed at NPS, a five-bladed model was developed that adheres to the basic principles of Robinson's Simplified Model. The MAPLE program along with its SIMULINK converted results can be found in Appendix B.

All of the energy expressions in the LaGrangian equation were broken into two terms either due to blade motion or fuselage motion.

$$T = T_F + \sum_{k=1}^{N} \left(T_B\right)_k$$

$$U = U_F + \sum_{k=1}^{N} \left(U_B\right)_k$$

$$D = D_F + \sum_{k=1}^{N} \left(D_B\right)_k$$

---

[2] For a thorough understanding of the modeler, the reader is encouraged to reference either Robinson's thesis [Ref. 4] or Robinson, Wood, and King's paper "FULL NONLINEAR SIMULATION OF COUPLED ROTOR/FUSELAGE RESPONSE USING SYMBOLICALLY DERIVED EQUATIONS OF MOTION", May 1998 [Ref. 7].

The essential standardization of the program lies in its synchronization of the coordinate systems. Five coordinate systems are utilized with transformations between the various systems based on Euler angle rotations. The coordinate systems are (1) inertial, (2) fuselage, (3) hub, (4) undeformed blade, and (5) deformed blade. The terms were eventually transformed to the inertial coordinate system and entered into a MAPLE worksheet designed to apply the LaGrangian equation [Ref. 4].

$$\vec{\rho} = \left(\vec{\rho}_{F\_I}\right)_I + \left(\vec{\rho}_{H\_F}\right)_I + \left(\vec{\rho}_{Bu\_H}\right)_I + \left(\vec{\rho}_{Bd\_Bu}\right)_I + \left(\vec{\rho}_{P\_Bd}\right)_I$$

$\vec{\rho}$ is the sum of relative positions with respect to various coordinate systems transformed to the inertial system

The generic simplified model presented in Robinson's thesis demonstrated a hypothetical aircraft's reaction to ground resonance. The task was to correlate the data prepared by Wood's report into the ground resonance modeler. The major obstacle presented was the fact the computer model provides translation at the rotor head in the lateral and longitudinal direction while Wood's model is a mass-spring-damper system of the landing gear in the roll and lateral modes only. The H-3 data had to be converted and manipulated to correspond to the inputs of the modeler. Therefore, all numbers initially given in Wood's report were solved for the landing gear model and then translated to the virtual point of rotation.

Essentially, the versatile modeler was converted to a one DOF modeler that isolated the desired individual modes. By increasing the longitudinal spring constant to a value several orders of magnitude larger than the actual spring constant of the lateral mode, the hub was effectively constrained for lateral motion only.
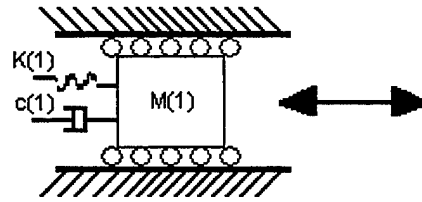
Figure 7. Block Diagram of Simulation Model

Isolating the time history output of the rotor hub was then evaluated for frequency
and damping. The Hilbert Transform method for determining damping was chosen over
the Moving Block technique because it was found to be more accurate for time histories
dominated by a single mode [Ref. 8]. Below is the Simulink diagram of the five-bladed
model representing the H-3.
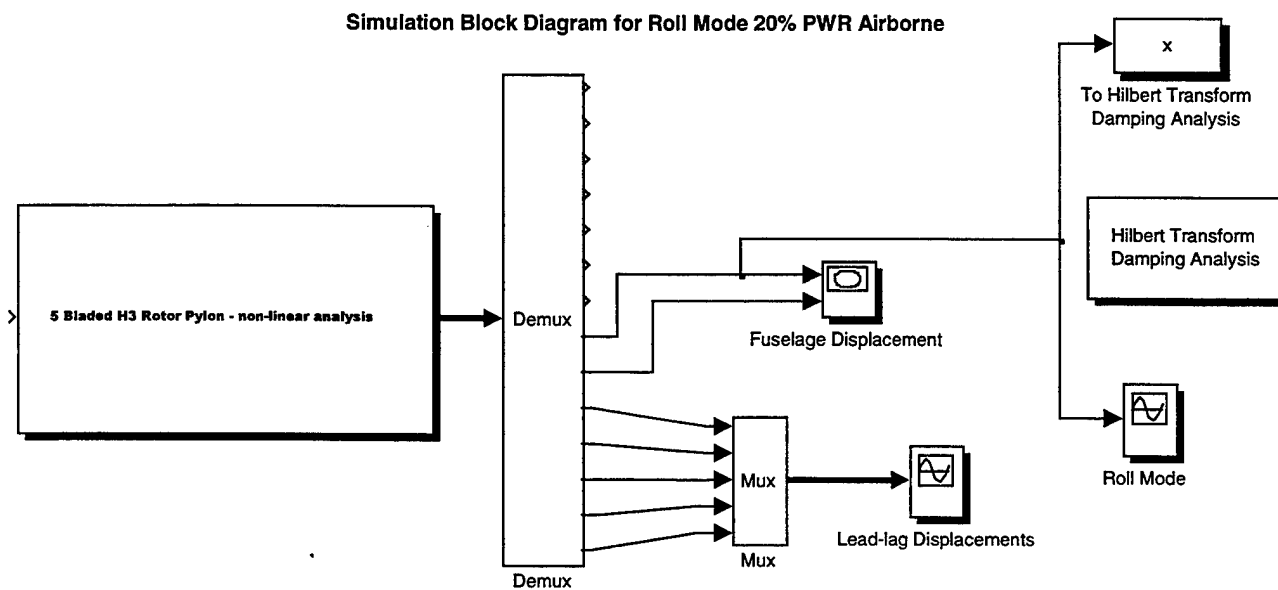
Figure 8. Simulink Diagram of 5 Blade NPS Modeler

B. PARAMETER INPUTS

Wood provides in his report many of the geometric values for the H-3. In order to conform all of the values to the modeler, some of the numbers required a simple conversion while others required a more complicated transformation about the point of virtual rotation. Table (4) is a list of all the parameter inputs necessary to run the Simulink block diagram [Ref. 4].

PARAMETER	PARAMETER SETTINGS	UNITS
Rotor Blade Mass	mb(1) mb(2) mb(3) mb(4) mb(5)	mass
Fuselage effective in x and y direction	M(1) M(2)	mass
Distance from hinge to center of mass of blade	R	length
Rotor Speed	Omega	rad/sec
Hinge Offset	e1	length
Angle at which lead-lag stops engage	z	radians
Azimuth phase angle of rotor blade	Phi(1) Phi(2) Phi(3) Phi(4) Phi(5)	radians
Lead-lag linear damping coefficient	Czeta(1) Czeta(2) Czeta(3) Czeta(4) Czeta(5)	moment/(rad/sec)
Lead-lag nonlinear damping coefficient	Vzeta(1) Vzeta(2) Vzeta(3) Vzeta(4) Vzeta(5)	moment/(rad/sec)^2
Fuselage linear damping coefficient in x and y direction	c(1) c(2)	force/(length/sec)
Fuselage nonlinear damping coefficient in x and y direction	v(1) v(2)	force/(length/sec)^2
Lead-lag linear spring coefficient	Ke(1) Ke(2) Ke(3) Ke(4) Ke(5)	moment/rad
Lead-lag nonlinear spring coefficient	Kd(1) Kd(2) Kd(3) Kd(4) Kd(5)	moment/rad^3
Lead-lag stop spring coefficient	Ks(1) Ks(2) Ks(3) Ks(4) Ks(5)	moment/rad
Effective fuselage stiffness in the x and y directions	K(1) K(2)	force/length
Fuselage states initial displacement conditions	xXi xYi	length
Fuselage states initial rate conditions	xrXi xrYi	length/sec
Blade states initial displacement conditions	x1i x2i x3i x4i x5i	rad
Blade states initial rate conditions	xr1i xr2i xr3i xr4i xr5i	rad/sec

Table 4. Parameter Inputs

The inputs that required special attention were the effective mass, the damping of the fuselage, the damping in the rotor head, and the spring constant of the fuselage. A short compilation of the conversion techniques is shown below. The reader is advised to reference Appendix C for a complete list of standard H-3 parameter values.

1. Fuselage Effective Mass in the x and y Directions – i.e. M(1)

This is similar to the conversion for the rotor blade mass. Depending upon which mode we're testing, M(1) will be set to M(2) because we've chosen an isotropic head.

2. Lead-Lag Linear Damping Coefficient – i.e. Czeta(1)

The effective damping coefficient of the blade about the drag hinge is solved by applying either Deutsch's criteria or using the theoretical data provided by Wood [Ref. 5]. Deutsch's criteria suggests the product of the damping in the pylon and blades must be essentially greater than or equal to Λ_3 or essentially the ratio of the effective mass of the blades to the combination of the effective mass of the blades and the pylon.

$$\Lambda_3 = \frac{1}{2}\left[\frac{nm}{(M+nm)}\right]\left[\frac{ml^2}{I_b}\right]$$

Deutsch's criteria will be addressed more thoroughly in section V. The Classics Revisited. Further, knowing the coefficient of damping in the pylon is equal to the coefficient of damping in the blades ($C_\theta = C_p$) from the Wood's derivation simplifies the solution.

$$\lambda_\phi = \frac{C_\phi}{I_b \omega_p}; \qquad \lambda_p = \frac{C_p}{I\omega_p}$$

$$\lambda_p \lambda_\phi \geq \frac{\Lambda_3}{(p-1)}$$

$$C_\phi = \frac{\Lambda_3 \omega_p^2}{C_\theta}\left[\frac{I \times I_b}{(p-1)}\right]$$

19

Figure (9), included in Wood's report depicts the empirical blade damping data of the
HSS-2 [Ref. 5].

Experimental Blade Damping of the H-3
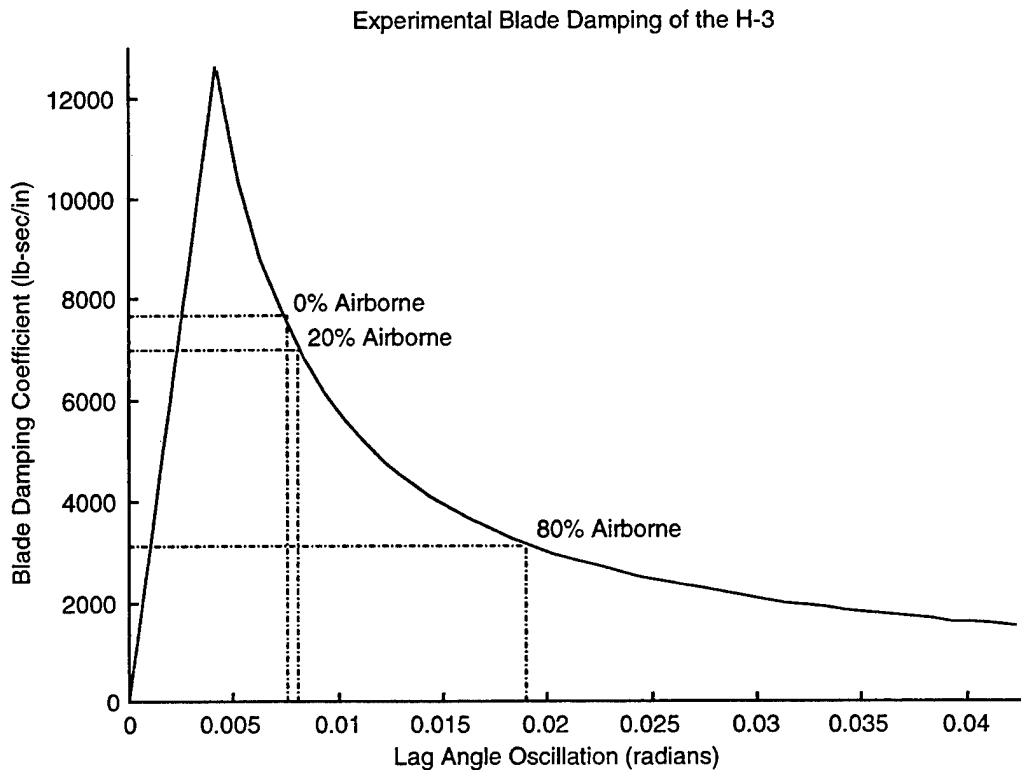
Figure 9. Blade Damping of H-3

3.   Fuselage Linear Damping Coefficient – C(1),C(2)

The linear damping coefficient in the roll mode was obtained through C_Θ. The
value at each power setting was transformed through the distance between the virtual
point of rotation for the roll mode and the height of the hub. Lateral damping of the
fuselage was calculated from a percentage of C_Θ. The lateral mode values of Θ/X for the
three power settings were used along with the damping results from the roll solutions to
obtain the estimated lateral damping of landing gear tires, structure and oleo.

4. Lead-Lag Linear Damping Coefficient – i.e. Ke(1), Ke(2), etc.

The linear lead-lag damping in the H-3 is zero because no springs are present in the rotor ($W_\Phi = 0$).

5. Effective Fuselage Stiffness in the x and y Directions – K(1), K(2)

The fuselage stiffness for the roll mode at three different power settings was calculated from the conversion of K_Θ. The value at each power setting was transformed through the distance between the virtual point of rotation for the roll mode and the height of the hub. K(1) assumed this value whereas K(2) was increased to a magnitude three orders of magnitude greater than K(1) to simulate the lateral motion only block model. For the lateral mode, the stiffness of the fuselage was taken from the original data given in Table (2) for K_{hhat}.

6. Fuselage States Initial Displacement Conditions – xXi, xYi

An initial displacement in the direction of the desired simulated motion served as an impetus to stimulated any possible divergence. xXi was set to 0.2 feet throughout the entire simulation.

IV.   SIMULATION RESULTS

A.   DISCUSSION

Once the simulation parameters for the H-3 were calculated, they were put into the Simulink block diagram H-3.mdl depicted in Figure (8). Located in Appendix C is a Parameter Setting and H-3 Value Chart listing all of the simulation parameter inputs. The output of the rotor hub becomes a Hilbert transform damping determination function which calculates frequency and damping from the time history plots. Simulink may also be used to visualize other information such as lead-lag response to fuselage perturbations as well as the dynamics of the model.

B.   ROLL MODE

The roll modes at the three power settings of 0/20/80 percent airborne were selected as the initial cases primarily because the uncoupled lateral mode has no damping in the Sikorsky report. At zero percent power, the modeler depicts the H-3 translation at the hub due to the fuselage roll as convergent with a frequency of 12.55 rad/sec.

Roll Mode-0% PWR Airborne
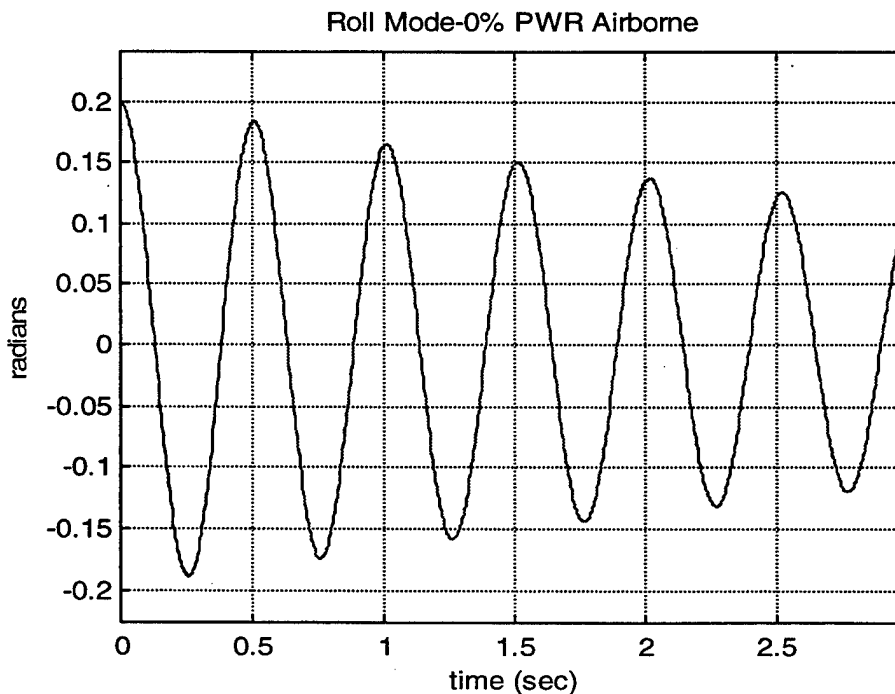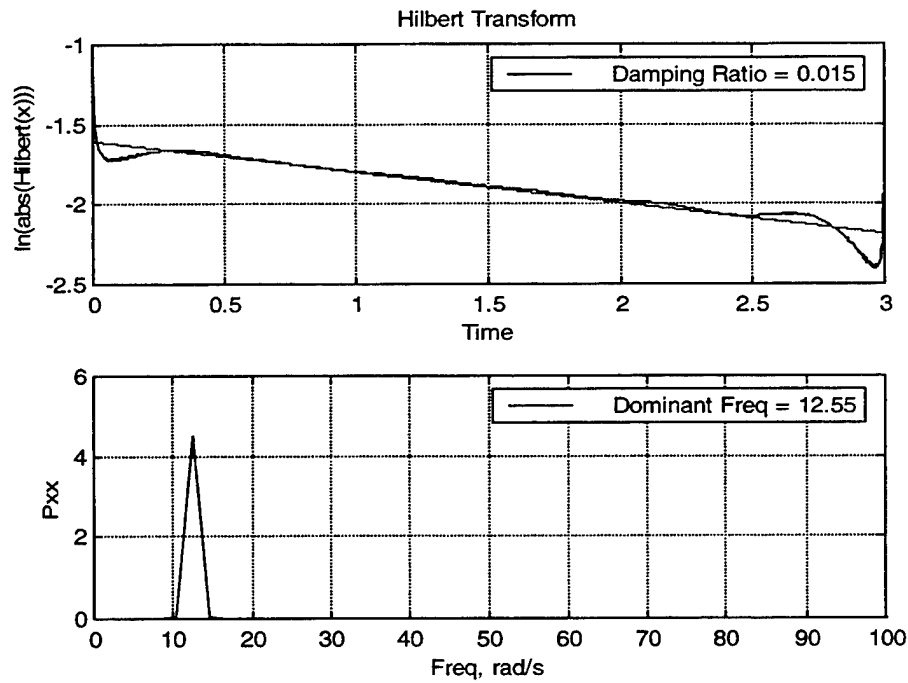
Figure 10. Roll Mode – 0% PWR Airborne

This frequency is similar to the regressive lag frequency calculated by Wood of 13.88 rad/sec. The ground resonance exciting frequency $W=\Omega\pm\omega_\phi$ is the combination of the rotational speed of the main rotor plus and minus the natural frequency of a rotating blade about its drag hinge. $\Omega+\omega_\phi$, the progressive lag mode, is well above any of the rigid body frequencies of the H-3, therefore as Coleman advises we can discard it and concern ourselves only with the modes likely to be excited, namely the regressive lag mode ($\Omega-\omega_\phi$). The damping ratio for the regressive lag mode in this case is was 0.015 showing no divergence.

Similarly, the modeler depicts the same stable trend in blade lag and lateral hub motion for the other two cases at twenty percent and eighty percent airborne power.
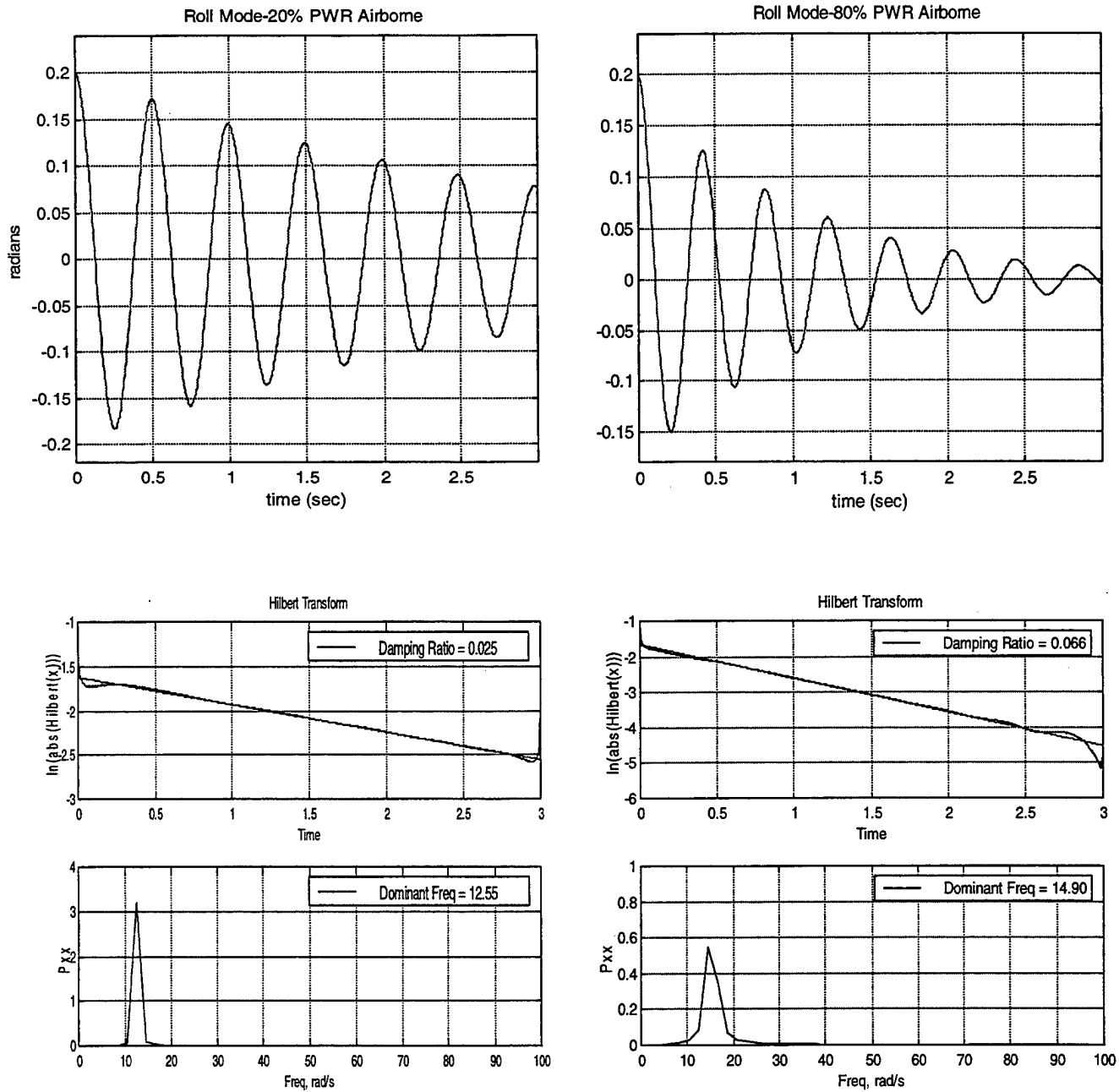
Figure 11. Roll Mode – 20% and 80 % PWR Airborne

Comparing the three power settings, it's evident by the increase in calculated damping ratios that the helicopter becomes a stiffer platform as power increases. Further, as power comes on the aircraft, the frequency seen at the hub rises slightly above the amount calculated by Wood.
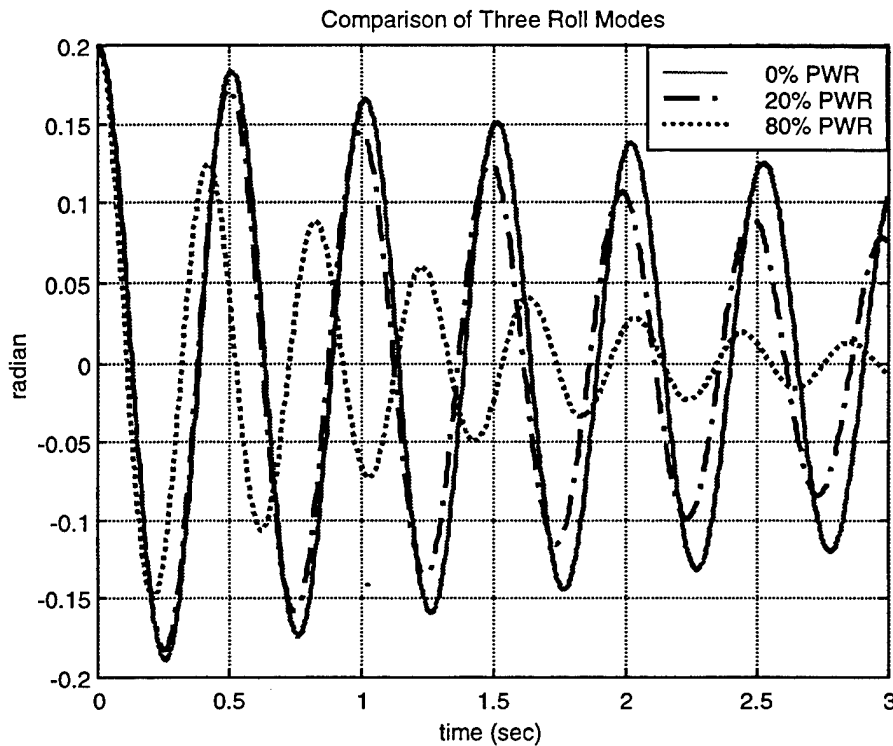
Figure 12. Comparison of Three Power Settings –Roll Mode

In agreement with Wood's results, the H-3 did not diverge in any of the normal operating cases. Therefore, as long as the H-3 is operating normally i.e. dampers operative, Nr in the normal operating range, and fuselage inertia within limits, the helicopter is free of ground resonance in the roll mode.

C.   LATERAL MODE

Damping in the lateral mode for Wood's model results from the roll-lateral coupling. The HSS-2 is configured for the fictitious case where as the roll-lateral coupling approaches zero, the lateral damping also goes to zero. Realistically, minimal damping in the lateral direction is provided by the tires and the structure of the landing gear itself. Since the data in the roll mode includes motion in both the lateral and vertical directions, all the numbers needed to simulate the lateral case are provided. From the ratio of the roll motion to the lateral translation or Θ/X, a percentage of damping of the lateral mode can be extracted from actual damping results in the aforementioned roll cases. Various models in each lateral mode case were run parametrically varying the damping value of the fuselage until the desired value of damping was achieved.

At zero percent power, the helicopter converges with the frequency at the hub equal to the same value as in the roll. The damping of 0.002 is a percentage of the value calculated from the roll case damping value of 0.015.
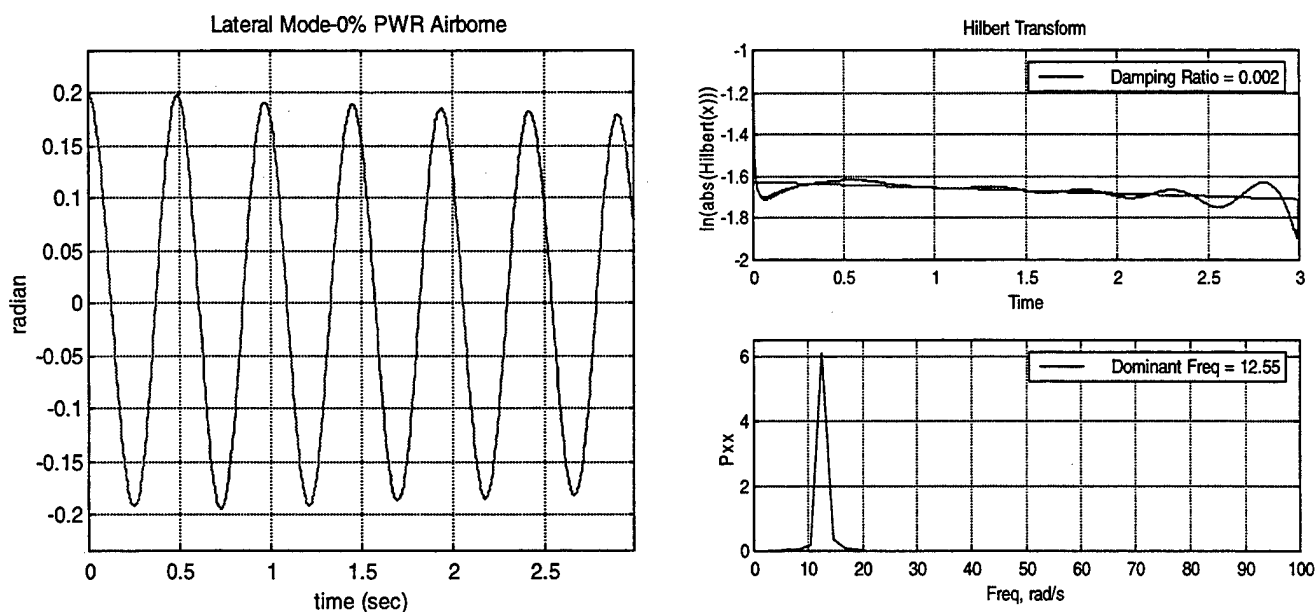
Figure 13. Lateral Mode – 0% PWR Airborne

27

The other two cases at twenty percent and eighty percent airborne power yield a similar trend as the zero percent airborne solution.
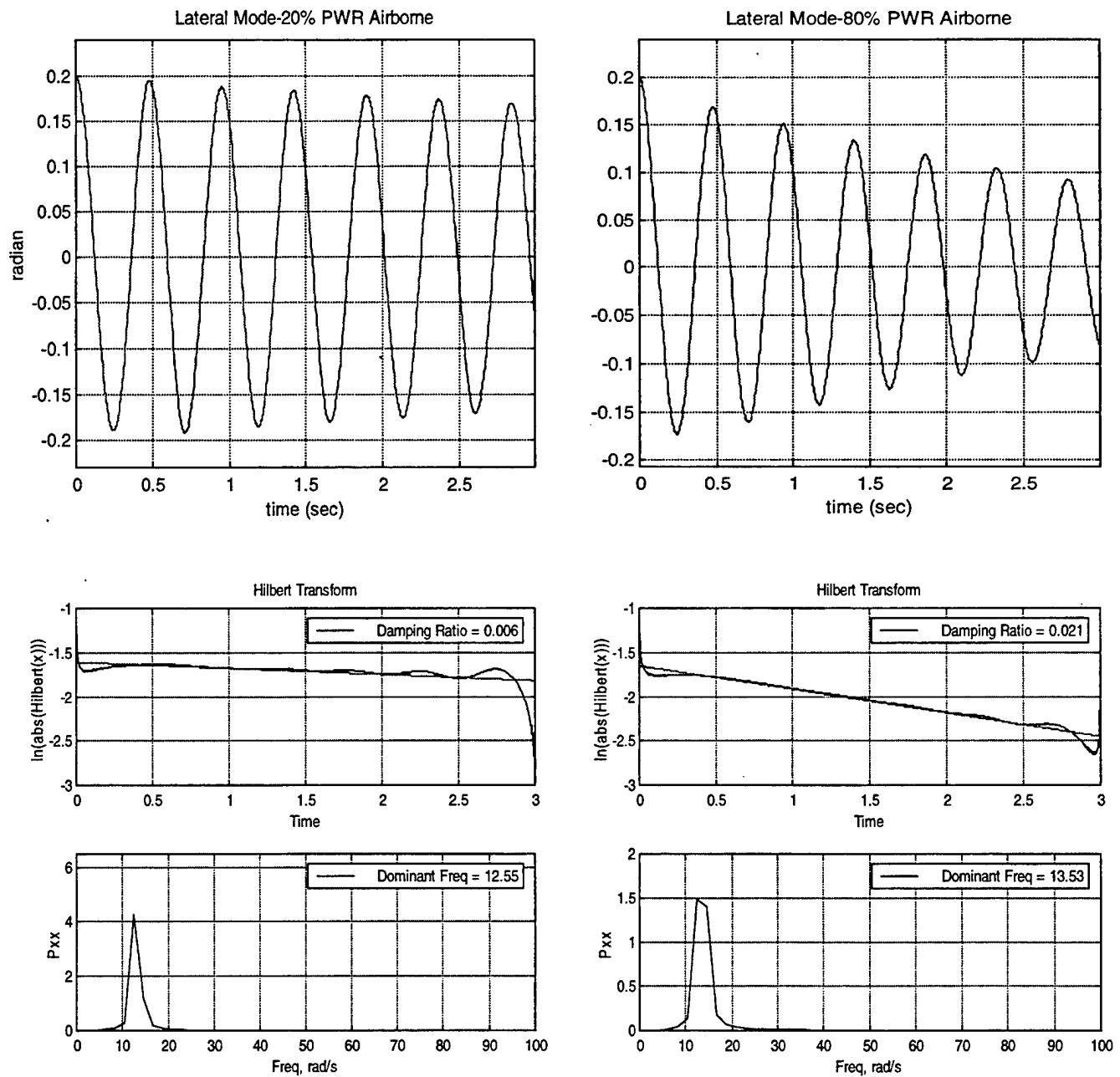
Figure 14. Lateral Mode – 20% and 80 % PWR Airborne

All three power settings demonstrated the stability of the H-3 throughout the range of the lateral mode. Similar to the roll mode, the three power settings show a trend toward a more stable platform. There is a small rise in the frequency of the hub in the eighty percent airborne calculation.

From the beginning, it was doubtful the lateral mode would allow divergent coupling of the rotor and rigid body frequencies since its frequencies were so small. The only probable time that the lateral mode could play a significant role in the onset of ground resonance is if the rotor rpm is slow enough to be in the lateral frequency range i.e. hesitation during run-up.

V. THE CLASSICS REVISITED

A. COLEMAN-FEINGOLD DISCUSSION

1. No Damping Case

In the classical report by Coleman and Feingold, it is noted that different types of vibrations are identified by the nature of the root of their characteristic equation. Specifically, the self-excited motion or "odd frequency" as they refer to it, is a vibration characterized by a complex number whose negative imaginary root represents negative damping [Ref. 1]. By nature, damping requires an external source of energy to be negative. Similar to Prouty's case 3 in his Stability and Control analysis, negative modeling requires a slight disturbance that will enable the helicopter to gain increasing energy with respect to time from the rotation of the rotor [Ref. 6]. Where,

$$m\ddot{x} + c\dot{x} + kx = 0$$
and
$$c < 0, \quad \frac{k}{m} > \left(\frac{c/2}{m}\right)^2$$

Coleman introduces a general model of a rotor with rigid blades free to hunt about the lag hinge that can be applied to any hinged aircraft with three or more blades. The purpose of the theory, as he points out, is to predict the occurrence of and show how to avoid self-excited vibrations. The theory teaches how to predict the natural frequencies and the unstable speed ranges in terms of certain physical parameters such as mass, stiffness, and length.

The characteristic equation obtained using LaGrange's equation is quite complicated with ω_f^2 to the fourth power and ω^2 to the second power. Recommendations are to first choose values for ω_f and solve for ω^2 without damping. Damping solutions can be added in later. The real part of the equation is plotted against ω for selected values of Λ_1, Λ_2, Λ_3, and s.

31

Where,

$$\Lambda_1 = \frac{e}{R} \quad \Lambda_2 = \frac{K_\varsigma}{I} \quad \Lambda_3 = \frac{nm_b}{2(M_p + nm_b)} \quad s = \frac{K_y}{K_x}$$

Figure (15) below, is a typical Coleman stability plot of ω_f versus ω for the real part of the characteristic equation without damping. The horizontal straight lines correspond to pylon bending and the slanting hyperbolas correspond to hinge deflection. Λ_3 is essentially the ratio of the effective mass of the rotor blades to the effective mass of the pylon. Naturally, a larger value of Λ_3 signifies an increase in energy of the rotor blades with relation to the pylon. Conversely, if Λ_3 were equal to zero, the blades have no effect on the pylon and the characteristic equation factors into equations yielding straight lines and hyperbolas, depicted as dash-dot lines below. Therefore, ground resonance is easier to attain as Λ_3 increases in value. In Figure (15), as Λ_3 increases, the intersections at the hyperbolas and straight lines begin to break off. The missing roots are complex conjugates and one of them has a negative imaginary part, which implies negative damping or a self-excited vibration [Ref. 1].
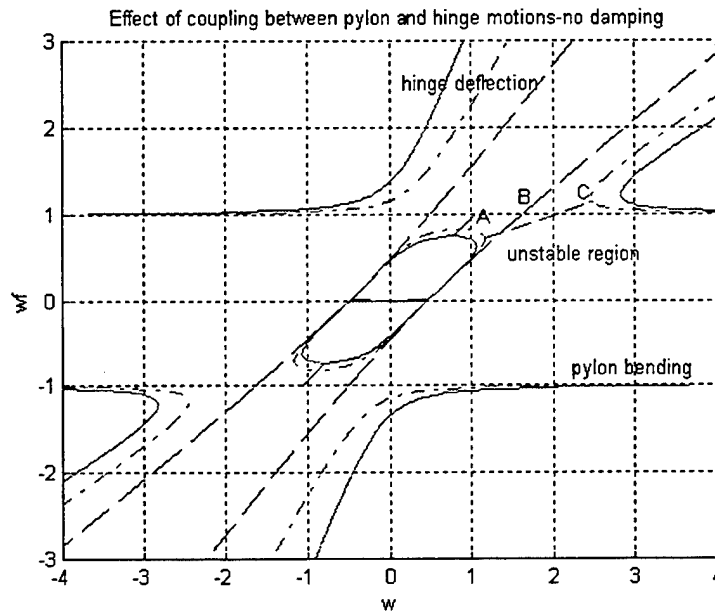
Figure 15. Typical Coleman Stability Plot

32

Point (A) represents the beginning of the self-excited range because the value of ω_f becomes complex at the value of ω where a vertical line is tangent to the plotted curve. At point (B), the motion again becomes stable only to become unstable again at point (C). Figure (16) is a corner plot specifically tailored to the H-3. It depicts the same trends as Coleman's stability plot in Figure (15).
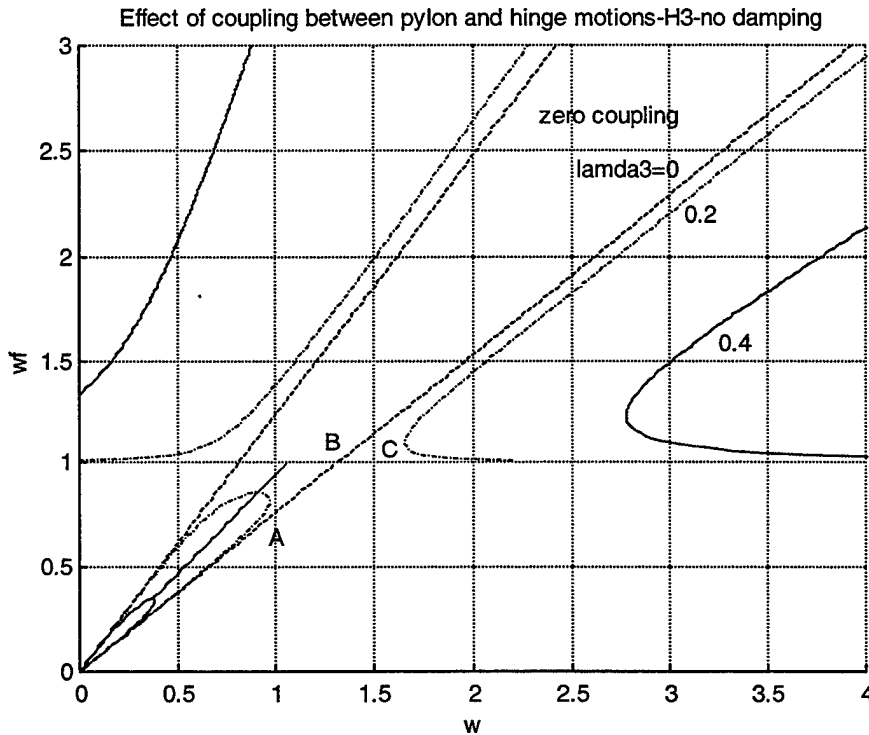
Figure 16. Corner Stability Plot of H-3

Since the most important information to obtain is the critical values of ω for the self-excited vibration range, Coleman prepared three charts that correspond to the three stiffness ratios (s=0,s=1,s=∞) that cover most rotorcraft. Instead of copying the stability charts themselves and depending upon a small deviation from Coleman's numbers, we've generated our own chart specific to the roll mode of the H-3 in Figure (17). Knowing the values of Λ_1, Λ_2, Λ_3, and s, Coleman's stability charts are generated by uncovering the critical ranges from the previous figures. The three lines in order of ascent are the lower limit of instability, the center of instability, and the upper limit of instability. Together, they bound the self-excited range or region of instability that the rotor head should avoid

without damping. Standard procedure is to draw a sloped line equal to $1/\omega\Lambda_1 + \Lambda_2$ similar to the one drawn in Figure (17). The line passes through all of the contours at the critical points of instability where $p = \Omega^2/\omega_p^2$. According to Wood, who used Coleman's generic curve, these p values in ascending order are 1.11, 1.31, and 1.60 [Ref. 5]. The p values in Figure (17) specific to the H-3 point to 1.0, 1.30 and 1.57.
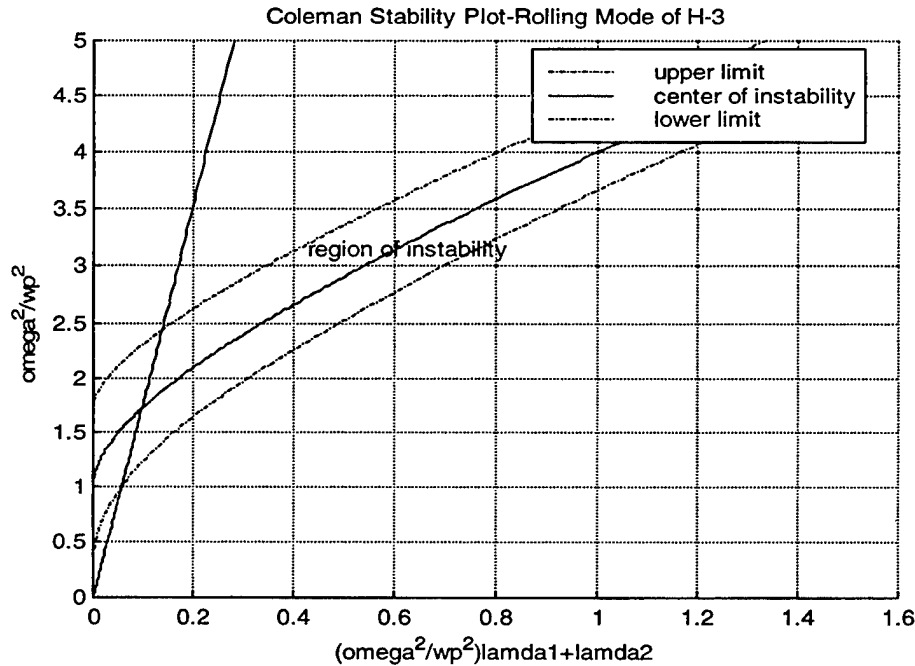
Figure 17. Coleman Stability Plot tailored to H-3

In Table (5), the corresponding critical H-3 rotor speeds at the three power settings for the roll mode are tabulated. The lateral mode was not considered in this exercise because its frequency was greatly below the regressive lag mode of the H-3.

	Center of Instability (rpm)		
Mode	0% Airborne	20% Airborne	80% Airborne
roll	221	215	208
	Range of Instability (rpm)		
Mode	0% Airborne	20% Airborne	80% Airborne
roll	170-267	165-259	160-252

Table 5. Critical Rotor Speeds

34

The NPS modeler was used to check the regions of instability for a case with no damping at the twenty percent airborne condition. Eliminating damping in the rotor head and body simulates Coleman's theory that there exists a range of rotor head speeds where divergent coupling occurs. Conversely, without damping, rotor speeds outside the ranges tabulated in Table (5) should converge.

At the H-3's normal operating rpm of 203 rpm, the helicopter was seen to diverge within seconds. Here, the damping ratio became negative allowing the instability to grow to catastrophic proportions after 3 seconds.
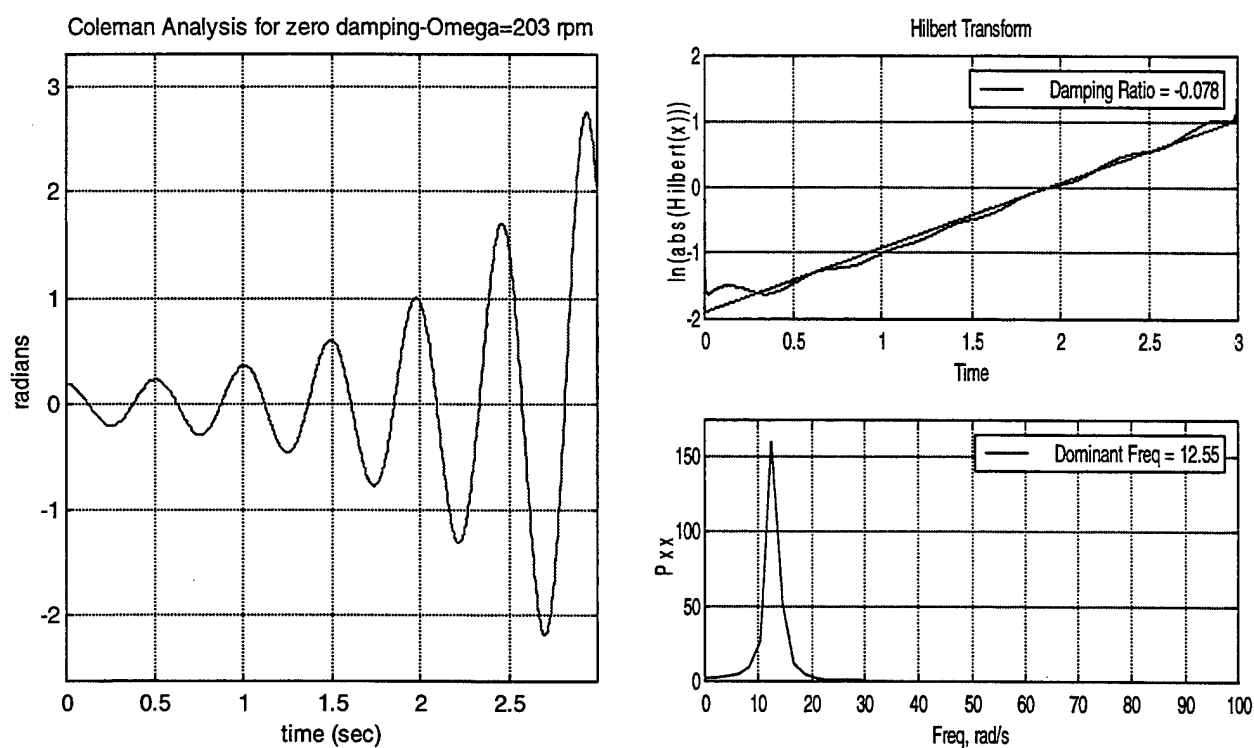
Figure 18. Center of Instability Test-Ω=203 rpm

Once the rpm of the main rotor is increased above the upper limit of the instability

range (Ω=280 rpm), the helicopter becomes neutrally stable.
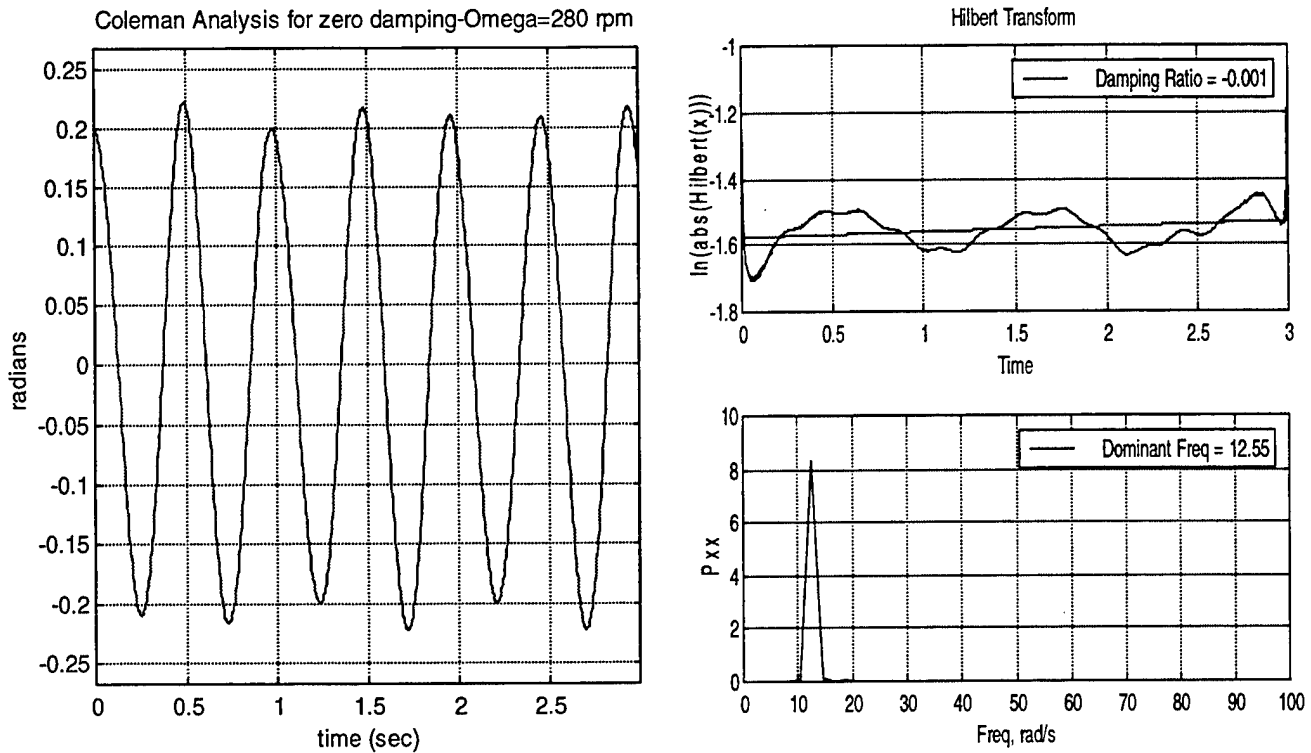
Figure 19. Upper Limit of Instability Test-Ω=280 rpm

Checking the lower limit of instability at Ω=140 rpm, the helicopter once again shows

a neutrally stable tendency. Of interesting note, the dominant frequency drops below the

standard modeler output of 12.55 rad/sec. In both the upper and lower limit range cases,

the damping ratio becomes so significantly small varying between negative and non-

negative numbers that a neutrally stable effect is seen in the time history plots.
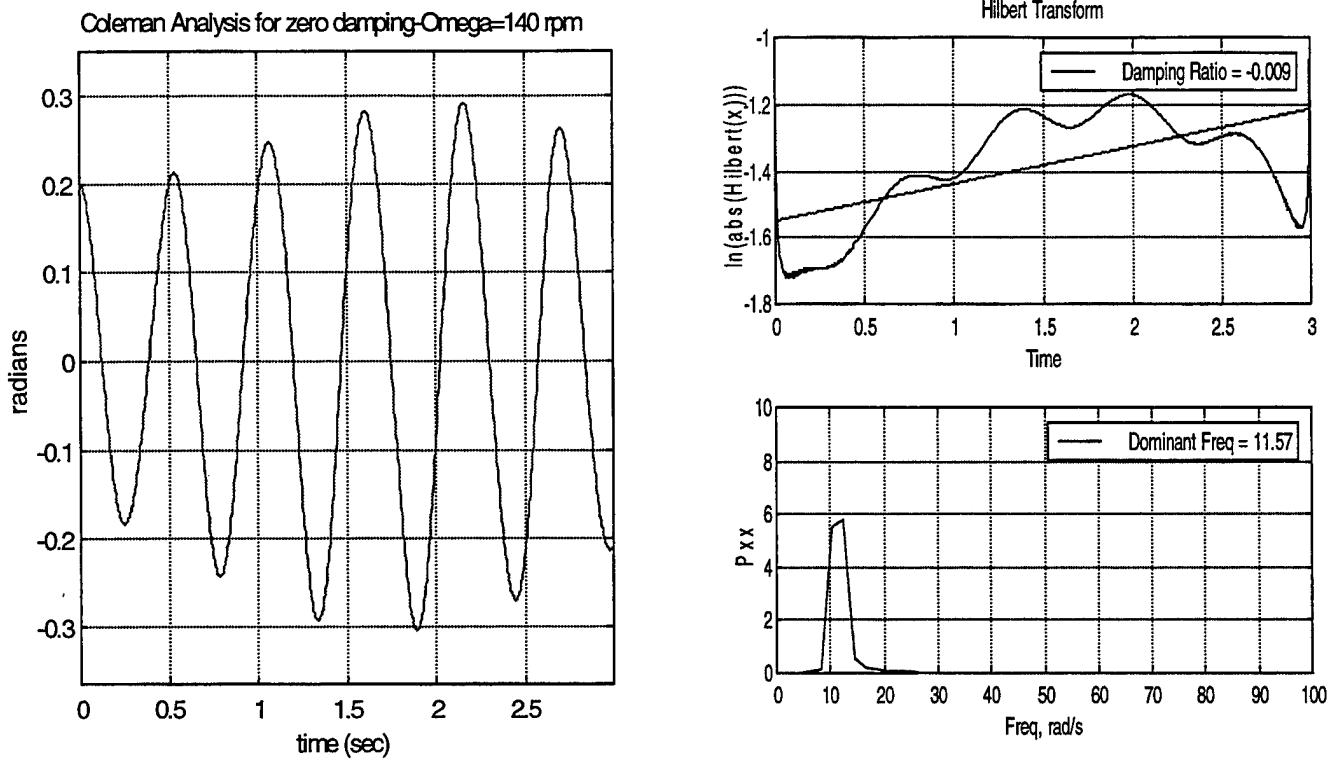
Figure 20. Lower Limit of Instability Test - Ω=140 rpm

2. Damping Case

Once an appreciation of the no damping scenario was obtained, the cases involving damping were evaluated. Coleman includes the effect of damping for two of his characteristic equations. The explicit form for the computation in the simplest case of isotropic supports with damping in the pylon and the hinges, but not in the rotating shaft (λ_a=0) is chosen from Coleman's equation (32) rearranged as follows [Ref. 1]:

For the real equation : $\omega^2 - 2B_R\omega + C_R = 0$ or $\omega = B_R \pm \sqrt{B_R - C_R}$

where $B_R = \dfrac{\omega_f}{1-\Lambda_1}\left[1+\dfrac{\lambda_p\lambda_\phi}{2\left(-\omega_f^2+\dfrac{K_f}{M}\right)}\right]$ and $C_R = -\dfrac{\omega_f^2}{1-\Lambda_1}\left(-1+\dfrac{\Lambda_2}{\omega_f^2}-\dfrac{\Lambda_3\omega_f^2+\lambda_p\lambda_\phi}{-\omega_f^2+\dfrac{K_f}{M}}\right)$

37

For the imaginary equation : $\omega^2 - 2B_I\omega + C_I = 0$ or $\omega = B_I \pm \sqrt{B_I - C_I}$

where $B_I = \dfrac{1}{1-\Lambda_1}\left[\omega_f - \dfrac{\lambda_\phi}{2\lambda_p\omega_f}\left(-\omega_f{}^2 + \dfrac{K_f}{M}\right)\right]$ and $C_I = -\dfrac{1}{1-\Lambda_1}\left(\dfrac{\lambda_\phi}{\lambda_p}\left(-\omega_f{}^2 + \dfrac{K_f}{M}\right) + \left(-\omega_f{}^2 + \Lambda_2\right)\right)$

Damping enters into the characteristic equation through the parameters λ_p =pylon damping and $\lambda_\phi \equiv$ blade damping. With the addition of damping, the problem is much like the one without damping except now the frequency equation has complex coefficients. This makes it impossible to plot the natural frequencies. The limits of the stability range are therefore found similar to that used in the subsonic flutter analysis. At a limit point between the stable and unstable regions ω_f is real. Therefore, the characteristic equation is broken into real and imaginary parts with ω_f considered real. So, the intersections of the real and imaginary equations give the rotor speeds and frequencies corresponding to the beginning and the end of the unstable band. A short program titled COLEMAN.m, located in Appendix D, shuffles through various ω_f 's using the simplified equation while solving for ω. The results for the H-3 with the damping product purposely reduced (λ_p=.059 and λ_ϕ=1.19) are plotted in Figure (21). A close up of the imaginary line crossing the center of instability at point B is shown in Figure (22).
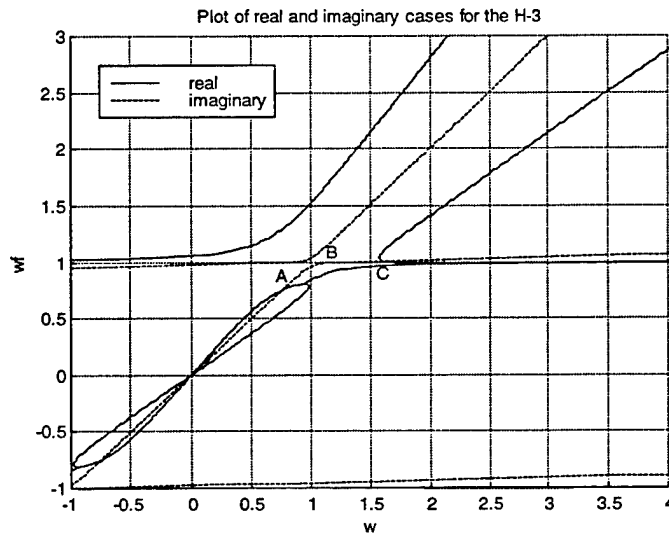
Figure 21. Real versus Imaginary Roots of Underdamped H-3

38
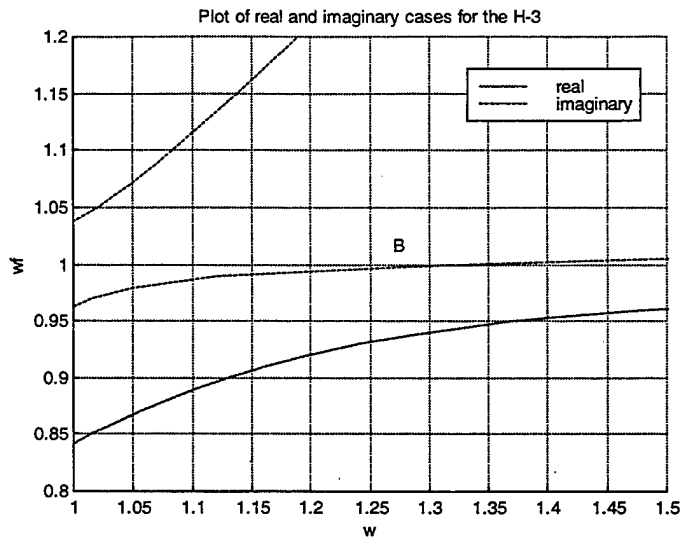
Figure 22. Close-up of Imaginary Root crossing at B

The three points (A,B,C) where the real and imaginary lines intersect one another in Figure (21) correspond to the lower, center and upper limits of instability for the H-3 with no damping. If a plot of the no damping case in Figure (16) was overlayed Figure (21), there would be very little difference between the two. Hence, Coleman's desire to present the easier no damping cases for general ground resonance usage.

B.   DEUTSCH'S CRITERIA

In their paper, Coleman and Feingold briefly touched upon how to eliminate the instability range of a helicopter. However, it was Deutsch who clarified and simplified the results of Coleman with respect to increasing the amount of damping until the gap between the limits of stability of the unstable region are finally eliminated. No matter what the values of damping are, the imaginary part of the equation will pass through the center of instability [Ref. 3]. This was evidenced in Figure (22) as the imaginary line crosses the center of instability at $\omega=1.3$.

The real part of the characteristic equation behaves as in the case with no damping. In Figure (15) and Figure (16), as the coupling between the pylon and the hinge increased i.e. Λ_3 is increased, the hyperbolas began to break away from the straight lines increasing the gap or instability region. Conversely, Deutsch claims as the product of the hub and

39

blade damping is increased, the real equations behave as the frequency curve without damping. When the coupling is decreased, the hyperbolas begin to move back toward the straight lines decreasing the instability region. Since the imaginary part will continue to cross at the center of instability, that means the real part will move toward the center of instability until the two lines intersect. Essentially, in order to remove the region of instability, the quantity of damping in the real part of the characteristic equation must allow for the real line to cross the center of instability.

The damping in the pylon and the hinge required to remove the region of instability is defined by Deutsch as follows:

$$\lambda_\phi = \frac{C_\phi}{I_b \omega_p}; \qquad \lambda_p = \frac{C_p}{I \omega_p}$$

$$\lambda_p \lambda_\phi > \frac{\Lambda_3}{(p-1)}$$

where

$$p = \frac{(1 + \sqrt{\Lambda_1 + \Lambda_2 - \Lambda_1 \Lambda_2})}{(1 - \Lambda_1)}$$

Knowing the values of Λ_1, Λ_2, Λ_3, and p, the damping product of the H-3 based upon Deutsch's criteria ($\lambda_p \lambda_\phi = 0.147$) is tabulated in Table (6).

Pct airborne	ω_p (rad/sec)	W (rad/sec)	Λ_3	C_θ (lb-in-sec)	C_ϕ (lb-sec/in)	λ_p	λ_ϕ	Damping product
0%	17.78	12.55	0.044	116079	1155839	0.045	3.305	0.147
20%	17.30	12.55	0.044	162377	782264	0.064	2.299	0.147
80%	16.79	13.35	0.044	327405	365429	0.133	1.107	0.147

Table 6. Damping Product in the Roll Mode

Adjusting the product values of the damping ratios in COLEMAN.m, a test of
Deustch's criteria is made. Figure (23) is a corner plot of the real and imaginary lines of
the H-3 similar to Figure (21), however, this time the pylon damping is increased from
$\lambda_p=.059$ to $\lambda_p=.09$ while the hub damping remained constant at $\lambda_\phi=1.19$. The gap is
beginning to close as the real frequency curves move toward the center of instability.
Although not plotted, the same results are evidenced if the hub damping is increased
while the pylon damping remains constant.

Plot of real and imaginary cases for the H-3
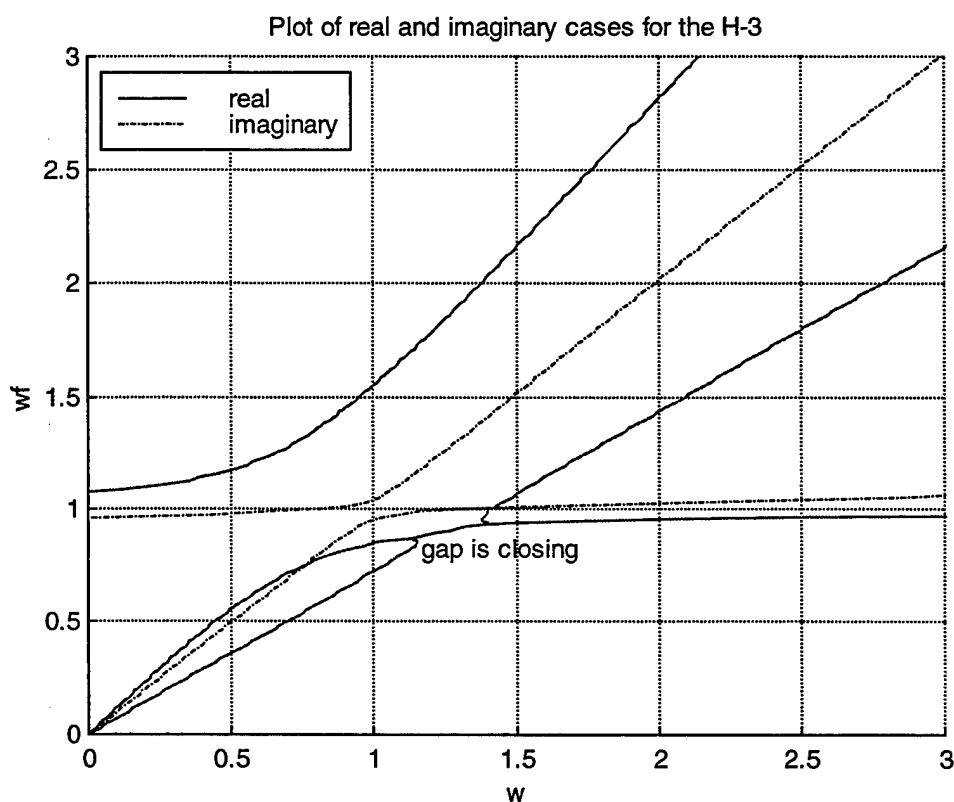
Figure 23. Test of Deutsch's Criteria for the H-3

41

The next plot Figure (24), is the result if the damping product is further increased. In this case, the pylon damping remained steady at $\lambda_p=.09$ while the hub damping increased to $\lambda_\phi=1.25$. The actual damping product ($\lambda_p\lambda_\phi=.113$) has now closed the instability gap in advance of Deutsch's criteria presented in Table (6). This minimal product of damping in the pylon and the hinge, will theoretically free the H-3 of ground resonance in the roll mode. Therefore, the damping products in Table (6) are conservative values incorporated as a factor of safety by the designers.
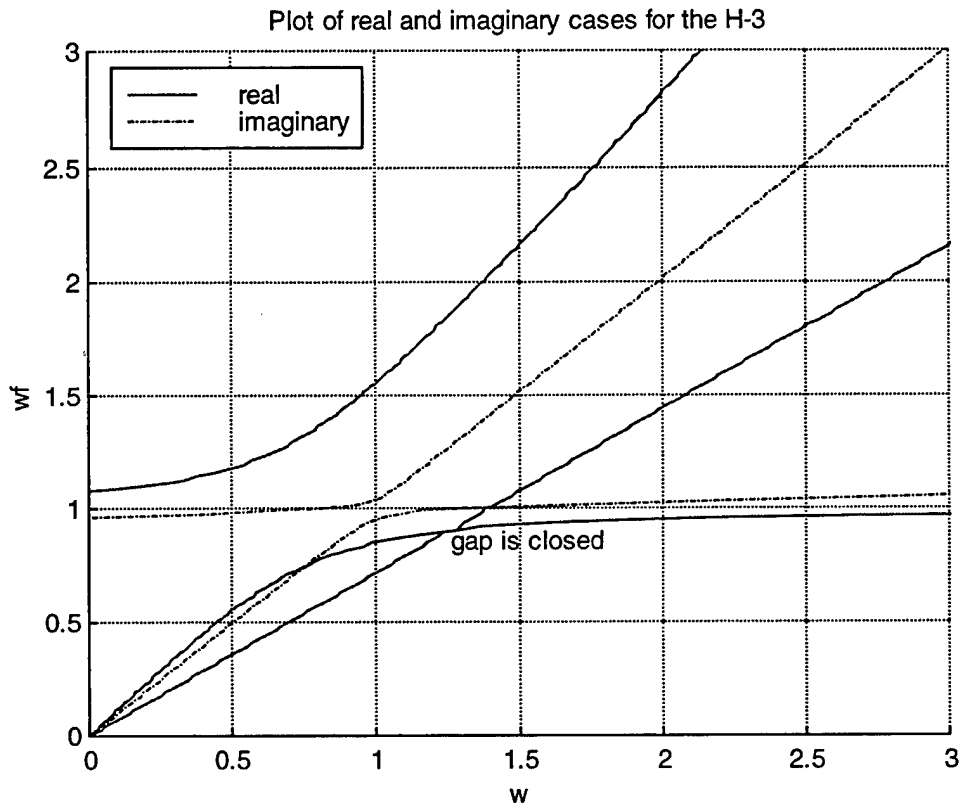
Figure 24. Approaching the Deutsch Criteria of the H-3

This point is further emphasized when a plot from Robinson's work is included [Ref. 5]. Figure (25) is a parametric plot of a simple model with an isotropic pylon and rotor. The damping ratio from the moving block result is plotted versus ω/ω_f for various Deutsch numbers. At a Deutsch number equal to one, the lowest point of the line does not touch the where the damping ratio is equivalent to zero. Robinson, therefore, also discovered a buffer or factor of safety prebuilt into Deutsch's criteria.
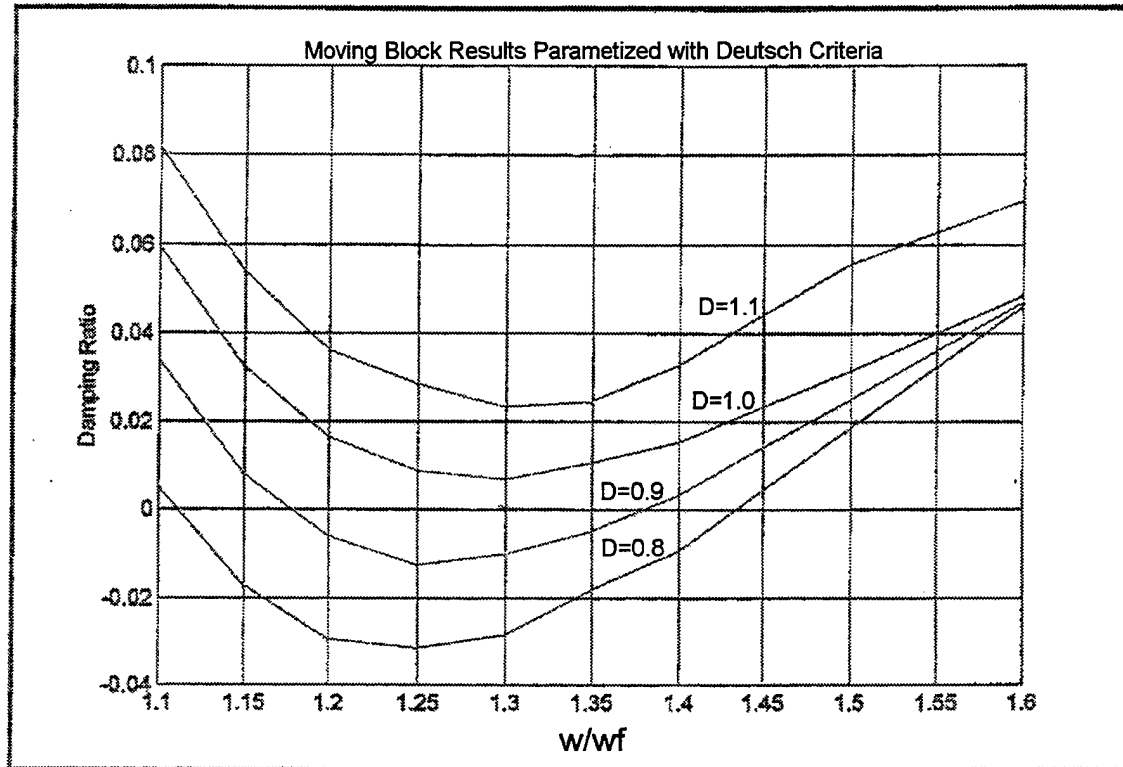
Figure 25. Robinson's Moving Block Results Parametized by Deutsch Number

Finally, the H-3 with its actual damping product ($\lambda_p\lambda_\phi$=0.147) is presented in Figure (26). Increasing the damping has actually forced the real line to split suggesting that the coupling between the pylon and hinge is well damped.

Plot of real and imaginary cases for the H-3
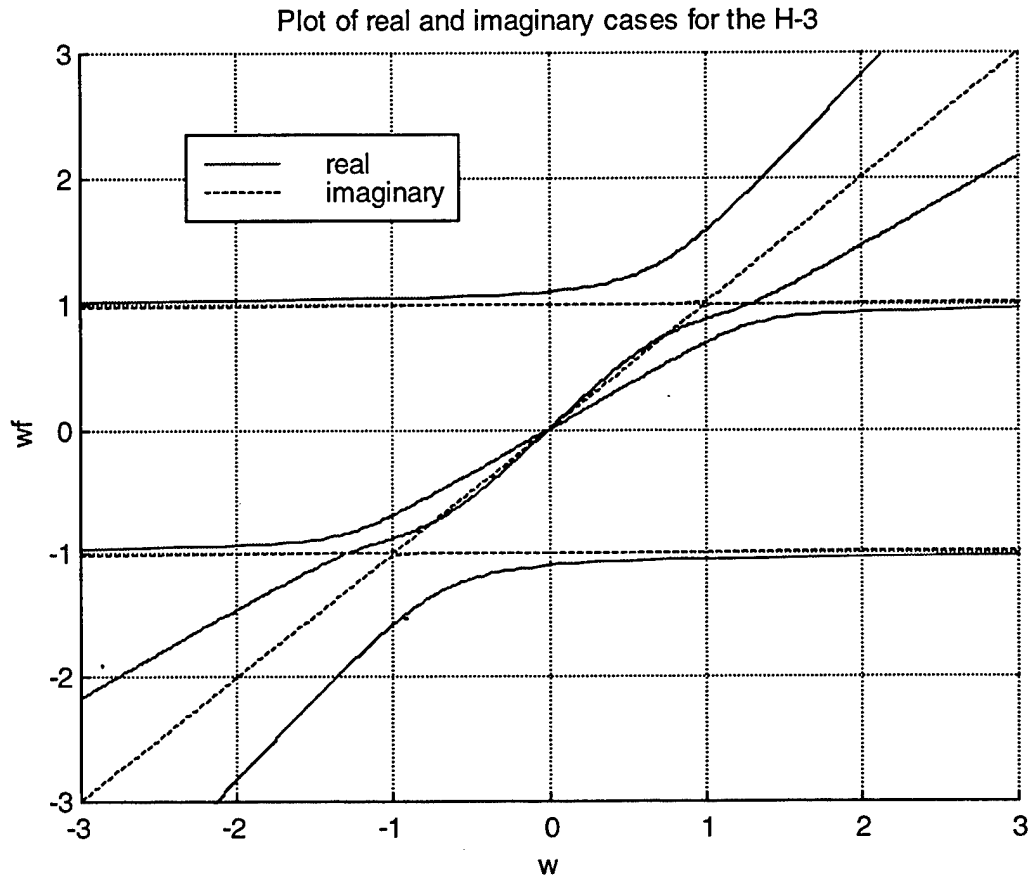
Figure 26. Plot of Real vs. Imaginary for the H-3

VI.   CONCLUSIONS AND RECOMMENDATIONS

A.   CONCLUSIONS

General insight into any ground resonance analysis can be obtained by examining the roll, lateral and in some cases the pitching mode of a rotorcraft. Just by the shear length of the H-3, the stable pitching mode was quickly eliminated permitting us to concentrate on the roll and lateral modes. For a generic five bladed rotorcraft, the pendular frequency of the blade transmits a force in to the fixed system at Ω-1/3Ω or 2/3Ω. This critical frequency, the regressive lag mode, can be close to the natural frequency in the helicopter's rigid body roll mode, as it is with the H-3. The natural frequency in the lateral mode was too low to couple with the rotor hub to cause any destabilizing motion. Nevertheless, we thoroughly examined the roll and lateral mode of the H-3 to link the classical work of Coleman, Feingold and Deutsch in the coupled rotor/fuselage field to the modern day computational techniques presented in this thesis.

Wood's H-3 model proved a valuable asset in formulating the correct parameters to enter into the NPS modeler. From the model, the virtual points of rotation for both modes were discovered. The coupled roll mode pivots about a point above the center of gravity whereas the coupled lateral mode rotates about a point underground. As power is brought on the aircraft, the points of virtual rotation increase until the helicopter breaks the ground and the rotation point climbs several rotor lengths above the helicopter. The virtual points of rotation were also used as a reference point about which the input parameters were calculated to correlate with the simulator.

The three power settings examined by Wood that were entered into the simulation model displayed the H-3 showed no tendency toward ground resonance in either the roll or lateral mode as its rigid body natural frequencies were changed while becoming partially airborne. The only possibility of the "light on the skids" analysis causing complications would be if an oleo strut or tire were improperly serviced by ground personnel or blown during a hard landing. Since the H-3 operates normally within the limits of instability at Ω=203 rpm, any reduction in damping could lead to a situation

45

similar to the divergent behavior depicted in Figure (18). For this reason, pilots and maintenance personnel should possess a general knowledge of ground resonance as well as an understanding of the aircraft's self-destructive potential.

The H-3 was designed to remain well clear of ground resonance by altering the parameters of the systems that govern the natural frequency and damping of the aircraft. A large portion of these calculations are thanks to the theoretical data published by Coleman, Feingold and Deutsch. Coleman and Feingold developed characteristic equations to define the instability envelope of a helicopter's rotor system with its rigid body modes. Wood's system placed into the NPS modeler defined the H-3's limits of instability similar to Coleman's own analysis. As previously stated, the normal operative rotor speed of the H-3 is within the band of instability. Above and below the limits of the band, the respective modes become neutrally stable. Due to the low rigid body natural frequency of the lateral mode, it is inconceivable that any coupling between the pylon and hinge would progress into ground resonance. The only possible time conceivable the two might destructively couple is if there is hesitation in increasing the rotor rpm during run-up.

At the disposal of the ground resonance designer, the proper manipulation of the product terms in Deutsch's criteria brings the real line back to the intersection of the imaginary line. The crossing occurs at the center of instability eliminating all ranges of divergence. Although it's a conservative value, increasing the damping to Deutsch's criteria also forces the real line to split suggesting that the coupling between the pylon and hinge is no longer unstable as when hyperbolas and straight lines where evidenced in the no damping case of Figure (15). Knowing Deutsch's criteria, the designer is free to choose blade dampers based upon the value of λ_ϕ whereas oleo damping is opted by considering λ_p. Other parameters in the designer's "toolbox" such as oleo spring rate, tire spring rate and landing gear tread width are also functioned into the damping product. Basically, as long as the product of the calculated damping parameters remain above the minimum to create an instability gap ($\lambda_\phi\lambda_p \approx 0.113$), the H-3 will be free of ground resonance at all rotor rpms.

With regard to NATOPS procedures, the corrective measure to suspected ground resonance is to immediately takeoff or if unable, shutdown [Ref. 9]. Since the H-3 is equipped with a rotor brake, both procedures instantaneously alter the natural frequency of the aircraft thereby changing the coupled modes between the fuselage and the rotor head. Considering the shutdown procedure may take a timely coordinated effort that the airframe just can't afford, the former procedure is the more preferred since it would only take a split second for either pilot to recognize the destabilizing mode and then apply collective to break the deck.

Previously, the lack of a modeler that could predict both the linear and non-linear portion of the stability characteristic curves required continued expensive and time consuming wind tunnel tests to confirm rotor/fuselage stability. Beside demonstrating the widespread applicability of the NPS modeler to a well known rotorcraft, continued development of this thesis may someday assist engineers in developing new airframes well clear of all ground resonance regimes.

B.   RECOMMENDATIONS

1.   A user-friendly simulation that eliminates the cut and paste procedure of the current modeler. For example, a modeler that is written strictly in MATLAB code vice MAPLE to Fortran to C etc.

2.   Ground resonance modeling of more recent aircraft especially ones currently in the developmental stage i.e. RAH-66 or CH-60.

3.   Examination of more degrees of freedom i.e. allow for flap in the blades.

4.   A detailed study on the design of helicopter damping based upon Deutsch's work.

5.   A study examining the air resonance of a modern day aircraft.

LIST OF REFERENCES

1.   Coleman, R. P., and Feingold, A. M., "Theory of Self Excited Mechanical Oscillations of Helicopter Rotors with Hinged Blades," NACA Report 1351, 1958.

2.   Feingold, A. M., "Theory of Mechanical Oscillations of Rotors with Two Hinged Blades," NACA ARR no. 3I13 Sept. 1943.

3.   Deutsch, M. L., "Ground Vibrations of Helicopters," Journal of Aeronautical Sciences, Vol. 15, No. 5, May 1946, pp. 223-228.

4.   Robinson, C. S., "Modeling and Analysis of Helicopter Ground Resonance Utilizing Symbolic Processing and Dynamic Simulation Software," Naval Postgraduate School, March 1997.

5.   Wood, E. R., "Preliminary Report on Mechanical Instability of HSS-2 Helicopters," Sikorsky Aircraft report no. SER-61163 Nov. 1958.

6.   Prouty, R. W., "Helicopter Performance, Stability, and Control," Krieger Publishing Company, Malabar, Fl., 1995, pp. 541-557.

7.   Robinson, C. S., Wood, E. R., King, R. L., "Full Nonlinear Simulation of Coupled Rotor/Fuselage Response Using Symbolically Derived Equations of Motion," AHS, May 1998.

8.   Wereley, N. M., and Smith, C. B., "Damping Identification in the Helicopter Rotor System," AHS, May 1998.

9.   NATOPS FLIGHT MANUAL SH-3D, NAVAIR 15 September 1988.

10. SIMULINK "Dynamic Simulation Software User's Guide," The MathWorks, Inc., 1992.

11. Hanselman D., and Littlefield B., "Mastering Matlab," Prentice Hall Upper Saddle River, N.J. 1995.

12. Matlab Help Desk, file://waverly/matlab$/help/helpdesk.html

13. Blachman, N. R., and Mossinghoff, M. J., "Maple V Quick Reference," Brooks/Cole Publishing Company, Pacific Grove, CA 1994.

14. Wood, E. R., "An Introduction to Helicopter Dynamics," AA3402 Helicopter Aerodynamics class notes 1998, pp 31-35.

15. Royal Air Force, http://www.airforce-technology.com/projects/seaking/specs.html

16. Helicopter Ground Resonance Event Summaries prepared by LCDR William Sass, Naval Safety Center H-60, H-3, H-2 Analyst

17. Gessow, A. and Meyers, G. C., "Aerodynamics of the Helicopter," 1985.

18. "Thesis Preparation Manual," Naval Postgraduate School, Monterey, CA Aug, 7, 1996.

APPENDIX A. SPRING RATE AND θ/X SOLUTION

1.   COUPLEDFREQ.M

```
%coupledfreq.m
%       The following program inputs the spring rate data from %Wood's
HSS-2 Report and then inputs that data into an %equation for Ktheta or
the spring in the roll mode.  An %eigenvalue/eigenvector problem is set
up that returns the %results for natural frequencies in the lateral and
roll %modes at three power settings of 0/20/80% airborne to the %file
naturalfreqs.txt.
%
close all
clear all
delete diary naturalfreqs.txt

diary on naturalfreqs.txt

Kh=[807 850 975];       % spring rate inputs
Kv=[1925 1875 1300];
Kd=[18500 18000 8000];
K2=[2967 1860 116];
Kht=[743 766 877];
Kvt=[1500 1475 1050];
omega=203;
Wphiprime=70.4;
W=omega-Wphiprime;
W=W*2*pi/60;
W=[W W W];
b=78;
a=[70.8 71.4 80.4];
C=[30 30 30];
Ml=42.06;
Ml=[Ml Ml Ml];
I=[146376 146376 146376];
Khprime=(2*Kh.*Kd)./(2*Kh+Kd)
Kvprime=2*Kv
Khhat=2*Khprime+Kht

Ktheta=2*Kvprime*b^2.*((K2.^2+K2.*Kvprime+C.^2.*W.^2))./((K2+Kvprime).^
2+ C.^2.*W.^2)...
+(2*a.^2.*Khprime+a.^2.*Kht)

Wpr2=0.5*(Khhat./Ml+Ktheta./I)+ 0.5*sqrt((Khhat./Ml-
Ktheta./I).^2+(4*Khhat.^2.*a.^2)./(I.*Ml));
Wpl2=0.5*(Khhat./Ml+Ktheta./I)- 0.5*sqrt((Khhat./Ml-
Ktheta./I).^2+(4*Khhat.^2.*a.^2)./(I.*Ml));

disp('The natural frequencies for roll at 0/20/80 percent power')
Wproll=sqrt(Wpr2)
disp('The natural frequencies for lateral motion at 0/20/80 percent
power')
```

51

```
Wplateral=sqrt(Wpl2)

disp('Setting up the eigenvector/eigenvalue problem')

A11=(Khhat./Ml);
A12=(Khhat./Ml).*a;
A21=(Khhat./I).*a;
A22=(Ktheta./I);
A=[A11,A12;A21,A22];

disp('Breaking up the A matrix into respective power settings')

PWR0=[A11(1) A12(1);A21(1) A22(1)];
disp('EV0 refers to the eigenvectors of the 0% power setting or ratio
of roll to lateral motion')
disp('eigen0 refers to the eigenvalues of wp^2 in roll and lateral
mode')
[EV0,eigen0]=eig(PWR0)

PWR20=[A11(2) A12(2);A21(2) A22(2)];
disp('EV20 refers to the eigenvectors of the 20% power setting')
disp('eigen20 refers to the eigenvalues of wp^2 in roll and lateral
mode')
[EV20,eigen20]=eig(PWR20)

PWR80=[A11(3) A12(3);A21(3) A22(3)];
disp('EV80 refers to the eigenvectors of the 80% power setting')
disp('eigen80 refers to the eigenvalues of wp^2 in roll and lateral
mode')
[EV80,eigen80]=eig(PWR80)

diary off
```

2.   NATURALFREQS.TXT

```
Khprime =

   1.0e+003 *

     1.4845    1.5533    1.5678


Kvprime =

        3850        3750        2600


Khhat =

   1.0e+003 *
```

```
     3.7120     3.8726     4.0127


Ktheta =

   1.0e+007 *

     3.9095     3.5038     2.7986

The natural frequencies for roll at 0/20/80 percent power

Wproll =

    17.7843    17.3002    16.7887

The natural frequencies for lateral motion at 0/20/80 percent power

Wplateral =

     6.2495     5.6698     2.1758

Setting up the eigenvector/eigenvalue problem
Breaking up the A matrix into respective power settings
EV0 refers to the eigenvectors of the 0% power setting or ratio of roll
to lateral motion
eigen0 refers to the eigenvalues of wp^2 in roll and lateral mode

EV0 =

   -1.0000    -0.9993
    0.0079    -0.0365

eigen0 =

    39.0560          0
          0   316.2819

EV20 refers to the eigenvectors of the 20% power setting
eigen20 refers to the eigenvalues of wp^2 in roll and lateral mode

EV20 =

   -1.0000    -0.9995
    0.0091    -0.0315

eigen20 =

    32.1466          0
          0   299.2984

EV80 refers to the eigenvectors of the 80% power setting
eigen80 refers to the eigenvalues of wp^2 in roll and lateral mode
```

53

```
EV80 =

    -0.9999   -0.9997
     0.0118   -0.0243

eigen80 =

    4.7341          0
         0   281.8613
```

1.   MAPLE PROGRAM

EQUATIONS OF MOTION FOR GROUND RESONANCE CONSIDERING ONLY INPLANE DEGREES OF FREEDOM

```
[ _____
[ DEFINE COORDINATE TRANSFORMATIONS
[ _____
[ Blade undeformed axis -- Hub :
[ > restart:
[ > with(linalg):
  Warning, new definition for norm
  Warning, new definition for trace
[ > psi:=Omega*t+Phi[k];
```

$$\psi := \Omega\, t + \Phi_k$$

```
[ > T1:=alpha->matrix(3,3,[1,0,0,0,cos(alpha),sin(alpha),0,-sin(alpha)
  ,cos(alpha)]);
```

$$T1 := \alpha \rightarrow \mathrm{matrix}(3, 3, [1, 0, 0, 0, \cos(\alpha), \sin(\alpha), 0, -\sin(\alpha), \cos(\alpha)])$$

```
[ > T2:=alpha->matrix(3,3,[cos(alpha),0,-sin(alpha),0,1,0,sin(alpha),0
  ,cos(alpha)]);
```

$$T2 := \alpha \rightarrow \mathrm{matrix}(3, 3, [\cos(\alpha), 0, -\sin(\alpha), 0, 1, 0, \sin(\alpha), 0, \cos(\alpha)])$$

```
[ > T3:=alpha->matrix(3,3,[cos(alpha),sin(alpha),0,-sin(alpha),cos(alp
  ha),0,0,0,1]);
```

$$T3 := \alpha \rightarrow \mathrm{matrix}(3, 3, [\cos(\alpha), \sin(\alpha), 0, -\sin(\alpha), \cos(\alpha), 0, 0, 0, 1])$$

```
[ > diff1:=arg->map(diff,arg,t);
```

$$diff1 := arg \rightarrow \mathrm{map}(diff, arg, t)$$

```
[ > M1:=transpose(T3(psi));
```

$$M1 := \begin{bmatrix} \cos(\Omega\, t + \Phi_k) & -\sin(\Omega\, t + \Phi_k) & 0 \\ \sin(\Omega\, t + \Phi_k) & \cos(\Omega\, t + \Phi_k) & 0 \\ 0 & 0 & 1 \end{bmatrix}$$

```
[ > M2:=transpose(T3(zeta[k](t)));
```

$$M2 := \begin{bmatrix} \cos(\zeta_k(t)) & -\sin(\zeta_k(t)) & 0 \\ \sin(\zeta_k(t)) & \cos(\zeta_k(t)) & 0 \\ 0 & 0 & 1 \end{bmatrix}$$

```
[ _____
[ Energy of rotor blades
[ _____
[ Kinetic energy of kth rotor blade (TBk)
[ ---------------------------------
[ > rhoHI_I:=vector([u[1](t),u[2](t),0]);
```

$$rhoHI\_I := [u_1(t), u_2(t), 0]$$

```
[ > rhoBuH:=vector([e1,0,0]);
```

$$rhoBuH := [eI, 0, 0]$$

```
> rhoBuH_I:=multiply(M1,rhoBuH);
```

$$rhoBuH\_I := [\cos(\Omega\, t + \Phi_k)\, eI, \sin(\Omega\, t + \Phi_k)\, eI, 0]$$

```
> rhoPBd:=vector([R,0,0]);
```

$$rhoPBd := [R, 0, 0]$$

```
> rhoPBd_I:=multiply(M1,M2,rhoPBd);
```

$$rhoPBd\_I := [(\cos(\Omega\, t + \Phi_k)\cos(\zeta_k(t)) - \sin(\Omega\, t + \Phi_k)\sin(\zeta_k(t)))\, R,$$
$$(\sin(\Omega\, t + \Phi_k)\cos(\zeta_k(t)) + \cos(\Omega\, t + \Phi_k)\sin(\zeta_k(t)))\, R, 0]$$

```
> rho:=map(simplify,matadd(rhoHI_I,matadd(rhoBuH_I,rhoPBd_I)));
```

$$\rho := [u_1(t) + \cos(\Omega\, t + \Phi_k)\, eI + R\cos(\Omega\, t + \Phi_k)\cos(\zeta_k(t)) - R\sin(\Omega\, t + \Phi_k)\sin(\zeta_k(t)),$$
$$u_2(t) + \sin(\Omega\, t + \Phi_k)\, eI + R\sin(\Omega\, t + \Phi_k)\cos(\zeta_k(t)) + R\cos(\Omega\, t + \Phi_k)\sin(\zeta_k(t)), 0]$$

```
> V:=diff1(rho);
```

$$V := \left[\left(\frac{\partial}{\partial t}u_1(t)\right) - \sin(\Omega\, t + \Phi_k)\,\Omega\, eI - R\sin(\Omega\, t + \Phi_k)\,\Omega\cos(\zeta_k(t))\right.$$
$$- R\cos(\Omega\, t + \Phi_k)\sin(\zeta_k(t))\left(\frac{\partial}{\partial t}\zeta_k(t)\right) - R\cos(\Omega\, t + \Phi_k)\,\Omega\sin(\zeta_k(t))$$
$$- R\sin(\Omega\, t + \Phi_k)\cos(\zeta_k(t))\left(\frac{\partial}{\partial t}\zeta_k(t)\right),\ \left(\frac{\partial}{\partial t}u_2(t)\right) + \cos(\Omega\, t + \Phi_k)\,\Omega\, eI$$
$$+ R\cos(\Omega\, t + \Phi_k)\,\Omega\cos(\zeta_k(t)) - R\sin(\Omega\, t + \Phi_k)\sin(\zeta_k(t))\left(\frac{\partial}{\partial t}\zeta_k(t)\right)$$
$$\left.- R\sin(\Omega\, t + \Phi_k)\,\Omega\sin(\zeta_k(t)) + R\cos(\Omega\, t + \Phi_k)\cos(\zeta_k(t))\left(\frac{\partial}{\partial t}\zeta_k(t)\right), 0\right]$$

```
> TBk:=1/2*mb[k]*(V[1]^2+V[2]^2);
```

$$TBk := \frac{1}{2}mb_k\left(\left(\left(\frac{\partial}{\partial t}u_1(t)\right) - \sin(\Omega\, t + \Phi_k)\,\Omega\, eI - R\sin(\Omega\, t + \Phi_k)\,\Omega\cos(\zeta_k(t))\right.\right.$$
$$- R\cos(\Omega\, t + \Phi_k)\sin(\zeta_k(t))\left(\frac{\partial}{\partial t}\zeta_k(t)\right) - R\cos(\Omega\, t + \Phi_k)\,\Omega\sin(\zeta_k(t))$$
$$\left.- R\sin(\Omega\, t + \Phi_k)\cos(\zeta_k(t))\left(\frac{\partial}{\partial t}\zeta_k(t)\right)\right)^2 + \left(\left(\frac{\partial}{\partial t}u_2(t)\right) + \cos(\Omega\, t + \Phi_k)\,\Omega\, eI\right.$$
$$+ R\cos(\Omega\, t + \Phi_k)\,\Omega\cos(\zeta_k(t)) - R\sin(\Omega\, t + \Phi_k)\sin(\zeta_k(t))\left(\frac{\partial}{\partial t}\zeta_k(t)\right)$$
$$\left.\left.- R\sin(\Omega\, t + \Phi_k)\,\Omega\sin(\zeta_k(t)) + R\cos(\Omega\, t + \Phi_k)\cos(\zeta_k(t))\left(\frac{\partial}{\partial t}\zeta_k(t)\right)\right)^2\right)$$

```
--------------------------------
Potential energy for kth blade (UBk)
--------------------------------
> UBk1:=1/2*Ke[k]*zeta[k](t)^2; #Linear Elastic Forces
```

$$UBk1 := \frac{1}{2} Ke_k \, \zeta_k(t)^2$$

> UBk2:=1/4*Kd[k]*zeta[k](t)^4; #Duffing Elastic Forces

$$UBk2 := \frac{1}{4} Kd_k \, \zeta_k(t)^4$$

> UBk3:=1/4*Ks[k]*signum(zeta[k](t)-z)*(zeta[k](t)^2+z^2-2*zeta[k](t
)*z)+1/4*Ks[k]*signum(zeta[k](t)+z)*(-zeta[k](t)^2-z^2-2*zeta[k](t
)*z)+1/2*Ks[k]*zeta[k](t)^2+1/2*Ks[k]*z^2;

$$UBk3 := \frac{1}{4} Ks_k \, \mathrm{signum}(\zeta_k(t)-z) \, (\zeta_k(t)^2 + z^2 - 2\,\zeta_k(t)\,z)$$

$$+ \frac{1}{4} Ks_k \, \mathrm{signum}(\zeta_k(t)+z) \, (-\zeta_k(t)^2 - z^2 - 2\,\zeta_k(t)\,z) + \frac{1}{2} Ks_k \, \zeta_k(t)^2 + \frac{1}{2} Ks_k \, z^2$$

[UBk:=UBk1+UBk2+UBk3;
> UBk:=UBk1+UBk2;

$$UBk := \frac{1}{2} Ke_k \, \zeta_k(t)^2 + \frac{1}{4} Kd_k \, \zeta_k(t)^4$$

[---------------------------------
[Dissapative function for kth blade (DBk)
[---------------------------------

> DBk:=1/2*Czeta[k]*(diff(zeta[k](t),t))^2+Vzeta[k]*(diff(zeta[k](t)
  ,t))^2*abs(diff(zeta[k](t),t));

$$DBk := \frac{1}{2} Czeta_k \left(\frac{\partial}{\partial t} \zeta_k(t)\right)^2 + Vzeta_k \left(\frac{\partial}{\partial t} \zeta_k(t)\right)^2 \left|\frac{\partial}{\partial t} \zeta_k(t)\right|$$

[───
[Energy of hub
[───
[Kinetic energy of hub (TH) / Potential energy of hub (UH) / Dissapative function of hub (DH)
[───

> TF:=1/2*M[1]*(diff(u[1](t),t))^2+1/2*M[2]*(diff(u[2](t),t))^2;

$$TF := \frac{1}{2} M_1 \left(\frac{\partial}{\partial t} u_1(t)\right)^2 + \frac{1}{2} M_2 \left(\frac{\partial}{\partial t} u_2(t)\right)^2$$

> UF:=1/2*K[1]*u[1](t)^2+1/2*K[2]*u[2](t)^2;

$$UF := \frac{1}{2} K_1 \, u_1(t)^2 + \frac{1}{2} K_2 \, u_2(t)^2$$

> DF:=1/2*c[1]*(diff(u[1](t),t))^2+1/2*c[2]*(diff(u[2](t),t))^2+1/2*
  v[1]*(diff(u[1](t),t))^2*abs(diff(u[1](t),t))+1/2*v[2]*(diff(u[2](
  t),t))^2*abs(diff(u[2](t),t));

$$DF := \frac{1}{2} c_1 \left(\frac{\partial}{\partial t} u_1(t)\right)^2 + \frac{1}{2} c_2 \left(\frac{\partial}{\partial t} u_2(t)\right)^2 + \frac{1}{2} v_1 \left(\frac{\partial}{\partial t} u_1(t)\right)^2 \left|\frac{\partial}{\partial t} u_1(t)\right| + \frac{1}{2} v_2 \left(\frac{\partial}{\partial t} u_2(t)\right)^2 \left|\frac{\partial}{\partial t} u_2(t)\right|$$

[_____

[Generalized forces on generalized displacements

[_____

[> F[1]:=0;
$$F_1 := 0$$

[> F[2]:=0;
$$F_2 := 0$$

[> F[3]:=u[1];
$$F_3 := u_1$$

[> F[4]:=u[2];
$$F_4 := u_2$$

[> F[5]:=u[3];
$$F_5 := u_3$$

[> F[6]:=u[4];
$$F_6 := u_4$$

[> F[7]:=u[5];
$$F_7 := u_5$$

[_____

[Derivation of equations of motion using Lagrange's equation

[_____

```
[ > DOFF:=[u[1](t),u[2](t)]:
[ > DOFB:=[zeta[1](t),zeta[2](t),zeta[3](t),zeta[4](t),zeta[5](t)]:
[ > DOF:=[op(DOFF),op(DOFB)]:
[ > dDOF:=diff1(DOF):
[ > ddDOF:=diff1(dDOF):
[ > setA:={}:setB:={}:setC:={}:
[ > setD:={}:setE:={}:setF:={}:
[ > DOFq:=[]:dDOFq:=[]:ddDOFq:=[]:
[ > for i from 1 to vectdim(DOF) do
  >    DOFq:=[op(DOFq),q[i]]:
  >    dDOFq:=[op(dDOFq),dq[i]]:
  >    ddDOFq:=[op(ddDOFq),ddq[i]]:
  >    setA:=setA union {ddDOF[i]=ddDOFq[i]}:
  >    setB:=setB union {dDOF[i]=dDOFq[i]}:
  >    setC:=setC union {DOF[i]=DOFq[i]}:
  >    setD:=setD union {ddDOFq[i]=ddDOF[i]}:
  >    setE:=setE union {dDOFq[i]=dDOF[i]}:
  >    setF:=setF union {DOFq[i]=DOF[i]}:
  > od:
[ > set1:=setA union setB union setC;
```

$$set1 := \{\frac{\partial}{\partial t}\zeta_2(t) = dq_4, \zeta_2(t) = q_4, \frac{\partial}{\partial t}\left(\frac{\partial}{\partial t}\zeta_2(t)\right) = ddq_4, \frac{\partial}{\partial t}\left(\frac{\partial}{\partial t}\zeta_3(t)\right) = ddq_5, u_2(t) = q_2, \zeta_3(t) = q_5,$$

$$\frac{\partial}{\partial t}\zeta_3(t) = dq_5, \frac{\partial}{\partial t}u_1(t) = dq_1, \frac{\partial}{\partial t}\left(\frac{\partial}{\partial t}u_1(t)\right) = ddq_1, \frac{\partial}{\partial t}\left(\frac{\partial}{\partial t}\zeta_4(t)\right) = ddq_6, \zeta_4(t) = q_6, \frac{\partial}{\partial t}\zeta_4(t) = dq_6,$$

$$u_1(t) = q_1, \frac{\partial}{\partial t}\left(\frac{\partial}{\partial t}\zeta_1(t)\right) = ddq_3, \frac{\partial}{\partial t}\zeta_5(t) = dq_7, \zeta_5(t) = q_7, \frac{\partial}{\partial t}\left(\frac{\partial}{\partial t}\zeta_5(t)\right) = ddq_7, \zeta_1(t) = q_3,$$

$$\frac{\partial}{\partial t}u_2(t) = dq_2, \frac{\partial}{\partial t}\zeta_1(t) = dq_3, \frac{\partial}{\partial t}\left(\frac{\partial}{\partial t}u_2(t)\right) = ddq_2\}$$

```
> set2:=setD union setE union setF;
```

$$set2 := \{dq_4 = \frac{\partial}{\partial t}\zeta_2(t), q_4 = \zeta_2(t), ddq_4 = \frac{\partial}{\partial t}\left(\frac{\partial}{\partial t}\zeta_2(t)\right), ddq_5 = \frac{\partial}{\partial t}\left(\frac{\partial}{\partial t}\zeta_3(t)\right), ddq_2 = \frac{\partial}{\partial t}\left(\frac{\partial}{\partial t}u_2(t)\right),$$

$$dq_5 = \frac{\partial}{\partial t}\zeta_3(t), q_5 = \zeta_3(t), dq_2 = \frac{\partial}{\partial t}u_2(t), q_2 = u_2(t), ddq_6 = \frac{\partial}{\partial t}\left(\frac{\partial}{\partial t}\zeta_4(t)\right), dq_6 = \frac{\partial}{\partial t}\zeta_4(t), q_7 = \zeta_5(t),$$

$$q_1 = u_1(t), dq_1 = \frac{\partial}{\partial t}u_1(t), q_6 = \zeta_4(t), ddq_7 = \frac{\partial}{\partial t}\left(\frac{\partial}{\partial t}\zeta_5(t)\right), ddq_1 = \frac{\partial}{\partial t}\left(\frac{\partial}{\partial t}u_1(t)\right),$$

$$ddq_3 = \frac{\partial}{\partial t}\left(\frac{\partial}{\partial t}\zeta_1(t)\right), dq_7 = \frac{\partial}{\partial t}\zeta_5(t), q_3 = \zeta_1(t), dq_3 = \frac{\partial}{\partial t}\zeta_1(t)\}$$

```
[ > T:=TF:
[ > U:=UF:
[ > D1:=DF:
[ > for i from 1 to vectdim(DOFB) do
[ >      T:=T+subs(k=i,TBk):
[ >      U:=U+subs(k=i,UBk):
[ >      D1:=D1+subs(k=i,DBk):
[ > od:
[ > Temp:=subs(set1,T):
[ > for i from 1 to vectdim(DOF) do
[ >       temp1:=diff(Temp,dDOFq[i]):
[ >       temp2:=subs(set2,temp1):
[ >       temp3:=diff(temp2,t):
[ >       L1:=subs(set1,temp3):
[ >       L2:=diff(Temp,DOFq[i]):
[ >       L3:=diff(subs(set1,U),DOFq[i]):
[ >       L4:=diff(subs(set1,D1),dDOFq[i]):
[ >       EOM[i]:=simplify(L1-L2+L3+L4-F[i]):
[ > od:
[ > setS:={signum(1,q[3]-z)=0,signum(1,q[4]-z)=0,signum(1,q[5]-z)=0,si
|   gnum(1,q[6]-z)=0,signum(1,q[7]-z)=0,signum(1,q[3]+z)=0,signum(1,q[
|   4]+z)=0,signum(1,q[5]+z)=0,signum(1,q[6]+z)=0,signum(1,q[7]+z)=0,a
|   bs(1,dq[1])=0,abs(1,dq[2])=0,abs(1,dq[3])=0,abs(1,dq[4])=0,abs(1,d
```

```
  q[5])=0,abs(1,dq[6])=0,abs(1,dq[7])=0}:
> A:=matrix(vectdim(DOF),vectdim(DOF));
```
$$A := \operatorname{array}(1 .. 7, 1 .. 7, [\ ])$$
```
> for i from 1 to vectdim(DOF) do
>     for j from 1 to vectdim(DOF) do
>         A[i,j]:=coeff(EOM[i],ddDOFq[j]):
>         A[i,j]:=subs(setS,A[i,j]):
>     od:
> od:
> Ax2dot:=multiply(A,ddDOFq):
> f:=array(1..vectdim(DOF));
```
$$f := \operatorname{array}(1 .. 7, [\ ])$$
```
> for i from 1 to vectdim(DOF) do
>     f[i]:=-simplify(EOM[i]-Ax2dot[i]):
>     f[i]:=subs(setS,f[i]):
> od:
> x1dot:=[]:x1:=[]:
> for i from 1 to vectdim(DOF) do x1dot:=[op(x1dot),x[i]] od:
> for i from vectdim(DOF)+1 to 2*vectdim(DOF) do x1:=[op(x1),x[i]]
>     od:
> setX:={}:
> for i from 1 to vectdim(DOF) do
>     setX:=setX union {dDOFq[i]=x1dot[i]}:
>     setX:=setX union {DOFq[i]=x1[i]}:
> od:
> interface(labelling=false);
> A1:=subs(setX ,op(A));
```
$AI :=$

$[mb_1 + mb_2 + mb_3 + mb_4 + mb_5 + M_1, 0,$

$-mb_1 R \cos(\Omega t + \Phi_1) \sin(x_{10}) - mb_1 R \sin(\Omega t + \Phi_1) \cos(x_{10}),$

$-mb_2 R \cos(\Omega t + \Phi_2) \sin(x_{11}) - mb_2 R \sin(\Omega t + \Phi_2) \cos(x_{11}),$

$-mb_3 R \sin(\Omega t + \Phi_3) \cos(x_{12}) - mb_3 R \cos(\Omega t + \Phi_3) \sin(x_{12}),$

$-mb_4 R \cos(\Omega t + \Phi_4) \sin(x_{13}) - mb_4 R \sin(\Omega t + \Phi_4) \cos(x_{13}),$

$-mb_5 R \cos(\Omega t + \Phi_5) \sin(x_{14}) - mb_5 R \sin(\Omega t + \Phi_5) \cos(x_{14})]$

$[0, mb_1 + mb_3 + mb_4 + mb_5 + mb_2 + M_2,$

$-mb_1 R \sin(\Omega t + \Phi_1) \sin(x_{10}) + mb_1 R \cos(\Omega t + \Phi_1) \cos(x_{10}),$

$-mb_2 R \sin(\Omega t + \Phi_2) \sin(x_{11}) + mb_2 R \cos(\Omega t + \Phi_2) \cos(x_{11}),$

$mb_3 R \cos(\Omega t + \Phi_3) \cos(x_{12}) - mb_3 R \sin(\Omega t + \Phi_3) \sin(x_{12}),$

$mb_4\,R\cos(\Omega\,t+\Phi_4)\cos(x_{13})-mb_4\,R\sin(\Omega\,t+\Phi_4)\sin(x_{13})\,,$

$-mb_5\,R\sin(\Omega\,t+\Phi_5)\sin(x_{14})+mb_5\,R\cos(\Omega\,t+\Phi_5)\cos(x_{14})]$

$[-mb_1\,R\cos(\Omega\,t+\Phi_1)\sin(x_{10})-mb_1\,R\sin(\Omega\,t+\Phi_1)\cos(x_{10})\,,$

$-mb_1\,R\sin(\Omega\,t+\Phi_1)\sin(x_{10})+mb_1\,R\cos(\Omega\,t+\Phi_1)\cos(x_{10})\,,mb_1\,R^2,0\,,0\,,0\,,0]$

$[-mb_2\,R\cos(\Omega\,t+\Phi_2)\sin(x_{11})-mb_2\,R\sin(\Omega\,t+\Phi_2)\cos(x_{11})\,,$

$-mb_2\,R\sin(\Omega\,t+\Phi_2)\sin(x_{11})+mb_2\,R\cos(\Omega\,t+\Phi_2)\cos(x_{11})\,,0\,,mb_2\,R^2,0\,,0\,,0]$

$[-mb_3\,R\sin(\Omega\,t+\Phi_3)\cos(x_{12})-mb_3\,R\cos(\Omega\,t+\Phi_3)\sin(x_{12})\,,$

$mb_3\,R\cos(\Omega\,t+\Phi_3)\cos(x_{12})-mb_3\,R\sin(\Omega\,t+\Phi_3)\sin(x_{12})\,,0\,,0\,,mb_3\,R^2,0\,,0]$

$[-mb_4\,R\cos(\Omega\,t+\Phi_4)\sin(x_{13})-mb_4\,R\sin(\Omega\,t+\Phi_4)\cos(x_{13})\,,$

$mb_4\,R\cos(\Omega\,t+\Phi_4)\cos(x_{13})-mb_4\,R\sin(\Omega\,t+\Phi_4)\sin(x_{13})\,,0\,,0\,,0\,,mb_4\,R^2,0]$

$[-mb_5\,R\cos(\Omega\,t+\Phi_5)\sin(x_{14})-mb_5\,R\sin(\Omega\,t+\Phi_5)\cos(x_{14})\,,$

$-mb_5\,R\sin(\Omega\,t+\Phi_5)\sin(x_{14})+mb_5\,R\cos(\Omega\,t+\Phi_5)\cos(x_{14})\,,0\,,0\,,0\,,0\,,mb_5\,R^2]$

```
> f1:=subs(setX ,op(f));
```

$f1 := [mb_5\cos(\Omega\,t+\Phi_5)\,\Omega^2\,el+mb_1\cos(\Omega\,t+\Phi_1)\,\Omega^2\,el+mb_2\cos(\Omega\,t+\Phi_2)\,\Omega^2\,el$

$\quad+mb_3\cos(\Omega\,t+\Phi_3)\,\Omega^2\,el+mb_4\cos(\Omega\,t+\Phi_4)\,\Omega^2\,el+mb_5\,R\cos(\Omega\,t+\Phi_5)\,\Omega^2\cos(x_{14})$

$\quad+2\,mb_4\,R\cos(\Omega\,t+\Phi_4)\,\Omega\cos(x_{13})\,x_6-mb_4\,R\sin(\Omega\,t+\Phi_4)\sin(x_{13})\,x_6^2$

$\quad-mb_4\,R\sin(\Omega\,t+\Phi_4)\,\Omega^2\sin(x_{13})-c_1\,x_1+mb_4\,R\cos(\Omega\,t+\Phi_4)\cos(x_{13})\,x_6^2$

$\quad-2\,mb_4\,R\sin(\Omega\,t+\Phi_4)\,\Omega\sin(x_{13})\,x_6+mb_4\,R\cos(\Omega\,t+\Phi_4)\,\Omega^2\cos(x_{13})$

$\quad+2\,mb_3\,R\cos(\Omega\,t+\Phi_3)\,\Omega\cos(x_{12})\,x_5-2\,mb_3\,R\sin(\Omega\,t+\Phi_3)\,\Omega\sin(x_{12})\,x_5$

$\quad-mb_3\,R\sin(\Omega\,t+\Phi_3)\sin(x_{12})\,x_5^2+2\,mb_2\,R\cos(\Omega\,t+\Phi_2)\,\Omega\cos(x_{11})\,x_4$

$\quad-2\,mb_2\,R\sin(\Omega\,t+\Phi_2)\,\Omega\sin(x_{11})\,x_4+2\,mb_1\,R\cos(\Omega\,t+\Phi_1)\,\Omega\cos(x_{10})\,x_3$

$\quad-mb_3\,R\sin(\Omega\,t+\Phi_3)\,\Omega^2\sin(x_{12})+mb_3\,R\cos(\Omega\,t+\Phi_3)\cos(x_{12})\,x_5^2-K_1\,x_8$

$\quad+mb_3\,R\cos(\Omega\,t+\Phi_3)\,\Omega^2\cos(x_{12})-mb_2\,R\sin(\Omega\,t+\Phi_2)\sin(x_{11})\,x_4^2$

$\quad-mb_2\,R\sin(\Omega\,t+\Phi_2)\,\Omega^2\sin(x_{11})+mb_2\,R\cos(\Omega\,t+\Phi_2)\cos(x_{11})\,x_4^2$

$\quad+mb_2\,R\cos(\Omega\,t+\Phi_2)\,\Omega^2\cos(x_{11})-2\,mb_1\,R\sin(\Omega\,t+\Phi_1)\,\Omega\sin(x_{10})\,x_3$

$\quad-mb_1\,R\sin(\Omega\,t+\Phi_1)\sin(x_{10})\,x_3^2-mb_1\,R\sin(\Omega\,t+\Phi_1)\,\Omega^2\sin(x_{10})$

$\quad+2\,mb_5\,R\cos(\Omega\,t+\Phi_5)\,\Omega\cos(x_{14})\,x_7+mb_1\,R\cos(\Omega\,t+\Phi_1)\cos(x_{10})\,x_3^2$

$\quad-2\,mb_5\,R\sin(\Omega\,t+\Phi_5)\,\Omega\sin(x_{14})\,x_7+mb_1\,R\cos(\Omega\,t+\Phi_1)\,\Omega^2\cos(x_{10})$

$\quad-mb_5\,R\sin(\Omega\,t+\Phi_5)\sin(x_{14})\,x_7^2-mb_5\,R\sin(\Omega\,t+\Phi_5)\,\Omega^2\sin(x_{14})$

$$+ mb_5 R \cos(\Omega t + \Phi_5) \cos(x_{14}) x_7^2 - v_1 x_1 |x_1|, -K_2 x_9 - c_2 x_2 + mb_3 R \sin(\Omega t + \Phi_3) \cos(x_{12}) x_5^2$$

$$+ mb_1 R \cos(\Omega t + \Phi_1) \sin(x_{10}) x_3^2 + mb_1 R \cos(\Omega t + \Phi_1) \Omega^2 \sin(x_{10})$$

$$+ 2 mb_2 R \cos(\Omega t + \Phi_2) \Omega \sin(x_{11}) x_4 + mb_1 R \sin(\Omega t + \Phi_1) \cos(x_{10}) x_3^2$$

$$+ mb_1 R \sin(\Omega t + \Phi_1) \Omega^2 \cos(x_{10}) + 2 mb_3 R \sin(\Omega t + \Phi_3) \Omega \cos(x_{12}) x_5$$

$$+ mb_2 R \cos(\Omega t + \Phi_2) \sin(x_{11}) x_4^2 + mb_2 R \cos(\Omega t + \Phi_2) \Omega^2 \sin(x_{11})$$

$$+ mb_2 R \sin(\Omega t + \Phi_2) \cos(x_{11}) x_4^2 + mb_3 R \cos(\Omega t + \Phi_3) \sin(x_{12}) x_5^2$$

$$+ mb_3 R \cos(\Omega t + \Phi_3) \Omega^2 \sin(x_{12}) + 2 mb_4 R \sin(\Omega t + \Phi_4) \Omega \cos(x_{13}) x_6$$

$$+ 2 mb_4 R \cos(\Omega t + \Phi_4) \Omega \sin(x_{13}) x_6 + 2 mb_3 R \cos(\Omega t + \Phi_3) \Omega \sin(x_{12}) x_5$$

$$+ mb_4 R \cos(\Omega t + \Phi_4) \Omega^2 \sin(x_{13}) + mb_4 R \sin(\Omega t + \Phi_4) \cos(x_{13}) x_6^2$$

$$+ mb_4 R \sin(\Omega t + \Phi_4) \Omega^2 \cos(x_{13}) + 2 mb_5 R \sin(\Omega t + \Phi_5) \Omega \cos(x_{14}) x_7$$

$$+ mb_2 R \sin(\Omega t + \Phi_2) \Omega^2 \cos(x_{11}) + 2 mb_5 R \cos(\Omega t + \Phi_5) \Omega \sin(x_{14}) x_7$$

$$+ mb_3 R \sin(\Omega t + \Phi_3) \Omega^2 \cos(x_{12}) + mb_5 R \cos(\Omega t + \Phi_5) \sin(x_{14}) x_7^2$$

$$+ 2 mb_1 R \sin(\Omega t + \Phi_1) \Omega \cos(x_{10}) x_3 + 2 mb_1 R \cos(\Omega t + \Phi_1) \Omega \sin(x_{10}) x_3$$

$$+ mb_5 R \cos(\Omega t + \Phi_5) \Omega^2 \sin(x_{14}) + mb_5 R \sin(\Omega t + \Phi_5) \cos(x_{14}) x_7^2$$

$$+ mb_5 R \sin(\Omega t + \Phi_5) \Omega^2 \cos(x_{14}) + 2 mb_2 R \sin(\Omega t + \Phi_2) \Omega \cos(x_{11}) x_4$$

$$+ mb_4 R \cos(\Omega t + \Phi_4) \sin(x_{13}) x_6^2 - v_2 x_2 |x_2| + mb_4 \sin(\Omega t + \Phi_4) \Omega^2 el$$

$$+ mb_2 \sin(\Omega t + \Phi_2) \Omega^2 el + mb_5 \sin(\Omega t + \Phi_5) \Omega^2 el + mb_3 \sin(\Omega t + \Phi_3) \Omega^2 el$$

$$+ mb_1 \sin(\Omega t + \Phi_1) \Omega^2 el,$$

$$u_1 - Czeta_1 x_3 - mb_1 \Omega^2 el R \sin(x_{10}) - Ke_1 x_{10} - Kd_1 x_{10}^3 - 2 Vzeta_1 x_3 |x_3|,$$

$$u_2 - Ke_2 x_{11} - Kd_2 x_{11}^3 - Czeta_2 x_4 - 2 Vzeta_2 x_4 |x_4| - mb_2 \Omega^2 el R \sin(x_{11}),$$

$$-mb_3 \Omega^2 el R \sin(x_{12}) - Czeta_3 x_5 + u_3 - Ke_3 x_{12} - Kd_3 x_{12}^3 - 2 Vzeta_3 x_5 |x_5|,$$

$$-2 Vzeta_4 x_6 |x_6| - mb_4 \Omega^2 el R \sin(x_{13}) - Czeta_4 x_6 - Ke_4 x_{13} - Kd_4 x_{13}^3 + u_4,$$

$$-mb_5 \Omega^2 el R \sin(x_{14}) + u_5 - Ke_5 x_{14} - 2 Vzeta_5 x_7 |x_7| - Kd_5 x_{14}^3 - Czeta_5 x_7]$$

```
[ > realib(fortran):
[ > B:=augment(A1,f1):
[ > fortran(B,optimized);
```

62

2. SIMULINK

The following program Blade5.m is the Matlab compatible cut and paste result from the above Maple program. It is the state space representation of the H-3 from the LaGrangian equation and is represented by the Simulink block diagram in figure (8).

```
function [sys, x0] = blade5(t,x,u,flag,I1,I2,I3,I4,I5,I6)
%
%    S-function arguments:
%    --------------------
%    t        =   time
%    x        =   state vector
%    u        =   input vector
%    flag     =   switch used by numerical integration (simulation)
%                 routine to access certain parts of the s-function
%
%    S-function input parameters:
%    ---------------------------
%
%    I1       =   [mb(1),mb(2),mb(3),mb(4),mb(5),M(1),M(2)]
%
%    I2       =   [R,Omega,e1,z]
%
%    I3       =   [Phi(1),Phi(2),Phi(3),Phi(4),Phi(5)]]
%
%    I4       =   [c(1),c(2),v(1),v(2),
%                   Czeta(1),Czeta(2),Czeta(3),Czeta(4),Czeta(5),
%                   Vzeta(1),Vzeta(2),Vzeta(3),Vzeta(4),Vzeta(5)]
%
%    I5       =   [Ke(1),Ke(2),Ke(3),Ke(4),Ke(5),
%                   Kd(1),Kd(2),Kd(3),Kd(4),Kd(5),
%                   Ks(1),Ks(2),Ks(3),Ks(4),Ks(5),
%                   K(1),K(2)]
%
%    I6       =   [xrXi,xrYi,xr1i,xr2i,xr3i,xr4i,xr5i,
%                   xXi,xYi,x1i,x2i,x3i,x4i,x5i]
%
% S-function to represent dynamics of 5 bladed coupled rotor-
% fuselage model which considers only inplane degrees of
% freedom, i.e., x and y translational fuselage degrees of freedom
% and lead-lag rotor blade degrees of freedom.
%
% Explaination of variables:
% -------------------------
%
% mb        ->      mass of blade
% M         ->      effective mass of fuselage
% R         ->      distance from lead-lag hinge to blade center of mass
% e1        ->      blade hinge offset
% Omega     ->      rotor speed
```

```
% z        ->     angle at which blade hits stops
% Phi      ->     blade phase angle w.r.t. azimuth postion
% c        ->     fuselage linear damping
% v        ->     fuselage hydraulic damping
% Czeta    ->     blade linear damping
% Vzeta    ->     blade non-linear dry friction damping
% K        ->     effective stiffness of fuselage (landing gear stiffness)
% Ke       ->     blade elastic spring constant
% Kd       ->     blade duffing spring constant
% Ks       ->     blade stop effective spring constant
% xr_ _i ->       initial rate
% x_ _i ->        initial displacement
%
%%%%%%%%%%%%%%%%%%%%%%%%%%%%%%%%%%%%%%%%%%%%%%%%%%%%%%%%%%%%%%%%%%%%%%%%%%
% Define input parameters
%%%%%%%%%%%%%%%%%%%%%%%%%%%%%%%%%%%%%%%%%%%%%%%%%%%%%%%%%%%%%%%%%%%%%%%%%%

mb=I1(1:5);
M=I1(6:7);
R=I2(1);
Omega=I2(2);
e1=I2(3);
z=I2(4);
Phi=I3;
c=I4(1:2);
v=I4(3:4);
Czeta=I4(5:9);
Vzeta=I4(10:14);
Ke=I5(1:5);
Kd=I5(6:10);
Ks=I5(11:15);
K=I5(16:17);
xrXi=I6(1);xrYi=I6(2);
xr1i=I6(3);xr2i=I6(4);xr3i=I6(5);xr4i=I6(6);xr5i=I6(7);
xXi=I6(8);xYi=I6(9);
x1i=I6(10);x2i=I6(11);x3i=I6(12);x4i=I6(13);x5i=I6(14);
%%%%%%%%%%%%%%%%%%%%%%%%%%%%%%%%%%%%%%%%%%%%%%%%%%%%%%%%%%%%%%%%%%%%%%%%%%
% S-function flag conditionals
%%%%%%%%%%%%%%%%%%%%%%%%%%%%%%%%%%%%%%%%%%%%%%%%%%%%%%%%%%%%%%%%%%%%%%%%%%
if flag == 0

        sys=[14,0,14,5,0,0];

x0=[xrXi,xrYi,xr1i,xr2i,xr3i,xr4i,xr5i,xXi,xYi,x1i,x2i,x3i,x4i,x5i];

elseif flag == 1

        t2 = mb(1)*R;
        t3 = Omega*t;
        t4 = t3+Phi(1);
        t5 = cos(t4);
        t6 = sin(x(10));
        t7 = t5*t6;
        t9 = sin(t4);
```

```
t10 = cos(x(10));
t11 = t9*t10;
t13 = -t2*t7-t2*t11;
t14 = mb(2)*R;
t15 = t3+Phi(2);
t16 = cos(t15);
t17 = sin(x(11));
t18 = t16*t17;
t20 = sin(t15);
t21 = cos(x(11));
t22 = t20*t21;
t24 = -t14*t18-t14*t22;
t25 = mb(3)*R;
t26 = t3+Phi(3);
t27 = sin(t26);
t28 = cos(x(12));
t29 = t27*t28;
t31 = cos(t26);
t32 = sin(x(12));
t33 = t31*t32;
t35 = -t25*t29-t25*t33;
t36 = mb(4)*R;
t37 = t3+Phi(4);
t38 = cos(t37);
t39 = sin(x(13));
t40 = t38*t39;
t42 = sin(t37);
t43 = cos(x(13));
t44 = t42*t43;
t46 = -t36*t40-t36*t44;
t47 = mb(5)*R;
t48 = t3+Phi(5);
t49 = cos(t48);
t50 = sin(x(14));
t51 = t49*t50;
t53 = sin(t48);
t54 = cos(x(14));
t55 = t53*t54;
t57 = -t47*t51-t47*t55;
t58 = Omega^2;
t59 = t49*t58;
t63 = t14*t16;
t65 = Omega*t21*x(4);
t67 = t36*t42;
t69 = Omega*t39*x(6);
t71 = t2*t5;
t73 = Omega*t10*x(3);
t75 = t27*t58;
t78 = t31*t58;
t81 = t31*t28;
t82 = x(5)^2;
t85 = t20*t17;
t86 = x(4)^2;
t89 = t20*t58;
```

```
t92 = t16*t58;
t95 = t9*t6;
t96 = x(3)^2;
t99 = t5*t10;
t102 = t47*t53;
t104 = Omega*t50*x(7);
t106 = t5*t58;
t109 = t53*t50;
t110 = x(7)^2;
t113 = t53*t58;
t116 = t49*t54;
t120 = t58*e1;
t122 = t47*t59*t54-K(1)*x(8)+2*t63*t65-2*t67*t69+2*t71*t73-
t25*t75*t32+t25*t78*t28+t25*t81*t82-t14*t85*t86-
t14*t89*t17+t14*t92*t21-t2*t95*t96+t2*t99*t96-2*t102*t104+t2*t106*t10-
t47*t109*t110-t47*t113*t50+t47*t116*t110+mb(1)*t5*t120;
t131 = t42*t39;
t132 = x(6)^2;
t135 = t36*t38;
t137 = Omega*t43*x(6);
t139 = t42*t58;
t145 = t38*t58;
t148 = t25*t31;
t150 = Omega*t28*x(5);
t152 = t38*t43;
t155 = t25*t27;
t157 = Omega*t32*x(5);
t160 = t27*t32;
t163 = t14*t20;
t165 = Omega*t17*x(4);
t167 = t2*t9;
t169 = Omega*t6*x(3);
t171 = t9*t58;
t174 = t47*t49;
t176 = Omega*t54*x(7);
t178 = t16*t21;
t181 =
mb(5)*t49*t120+mb(2)*t16*t120+mb(3)*t31*t120+mb(4)*t38*t120-
t36*t131*t132+2*t135*t137-t36*t139*t39-
v(1)*x(1)*abs(x(1))+t36*t145*t43+2*t148*t150+t36*t152*t132-2*t155*t157-
c(1)*x(1)-t25*t160*t82-2*t163*t165-2*t167*t169-
t2*t171*t6+2*t174*t176+t14*t178*t86;
t186 = -t2*t95+t2*t99;
t189 = -t14*t85+t14*t178;
t192 = t25*t81-t25*t160;
t195 = t36*t152-t36*t131;
t198 = -t47*t109+t47*t116;
t233 =
mb(4)*t42*t120+t25*t33*t82+2*t71*t169+t47*t51*t110+t47*t59*t50+t47*t55*
t110+t47*t113*t54+t36*t40*t132+2*t163*t65-
c(2)*x(2)+t25*t29*t82+mb(2)*t20*t120+mb(5)*t53*t120+mb(3)*t27*t120-
K(2)*x(9)+mb(1)*t9*t120+t2*t106*t6+t2*t7*t96+t2*t11*t96;
t265 =
2*t63*t165+t2*t171*t10+2*t155*t150+t14*t18*t86+t14*t92*t17+t14*t22*t86+
```

```
t25*t78*t32+2*t135*t69+2*t67*t137+2*t148*t157+t36*t145*t39+t36*t139*t43
+t36*t44*t132+2*t102*t176+t14*t89*t21+t25*t75*t28+2*t174*t104-
v(2)*x(2)*abs(x(2))+2*t167*t73;
        t267 = R^2;
        t271 = e1*R;
        t275 = x(10)^2;
        t284 = x(11)^2;
        t301 = x(12)^2;
        t317 = x(13)^2;
        t329 = x(14)^2;
        B(1,1) = mb(1)+mb(2)+mb(3)+mb(4)+mb(5)+M(1);
        B(1,2) = 0;
        B(1,3) = t13;
        B(1,4) = t24;
        B(1,5) = t35;
        B(1,6) = t46;
        B(1,7) = t57;
        B(1,8) = t122+t181;
        B(2,1) = 0;
        B(2,2) = mb(1)+mb(3)+mb(4)+mb(5)+mb(2)+M(2);
        B(2,3) = t186;
        B(2,4) = t189;
        B(2,5) = t192;
        B(2,6) = t195;
        B(2,7) = t198;
        B(2,8) = t233+t265;
        B(3,1) = t13;
        B(3,2) = t186;
        B(3,3) = mb(1)*t267;
        B(3,4) = 0;
        B(3,5) = 0;
        B(3,6) = 0;
        B(3,7) = 0;
        B(3,8) = u(1)-Czeta(1)*x(3)-mb(1)*t58*t271*t6-Ke(1)*x(10)-
Kd(1)*t275*x(10)-2*Vzeta(1)*x(3)*abs(x(3));
        B(4,1) = t24;
        B(4,2) = t189;
        B(4,3) = 0;
        B(4,4) = mb(2)*t267;
        B(4,5) = 0;
        B(4,6) = 0;
        B(4,7) = 0;
        B(4,8) = u(2)-Ke(2)*x(11)-Kd(2)*t284*x(11)-Czeta(2)*x(4)-
2*Vzeta(2)*x(4)*abs(x(4))-mb(2)*t58*t271*t17;
        B(5,1) = t35;
        B(5,2) = t192;
        B(5,3) = 0;
        B(5,4) = 0;
        B(5,5) = mb(3)*t267;
        B(5,6) = 0;
        B(5,7) = 0;
        B(5,8) = -mb(3)*t58*t271*t32-Czeta(3)*x(5)+u(3)-Ke(3)*x(12)-
Kd(3)*t301*x(12)-2*Vzeta(3)*x(5)*abs(x(5));
        B(6,1) = t46;
```

```matlab
        B(6,2)  = t195;
        B(6,3)  = 0;
        B(6,4)  = 0;
        B(6,5)  = 0;
        B(6,6)  = mb(4)*t267;
        B(6,7)  = 0;
        B(6,8)  = -2*Vzeta(4)*x(6)*abs(x(6))-mb(4)*t58*t271*t39-
Czeta(4)*x(6)-Ke(4)*x(13)-Kd(4)*t317*x(13)+u(4);
        B(7,1)  = t57;
        B(7,2)  = t198;
        B(7,3)  = 0;
        B(7,4)  = 0;
        B(7,5)  = 0;
        B(7,6)  = 0;
        B(7,7)  = mb(5)*t267;
        B(7,8)  = -mb(5)*t58*t271*t50+u(5)-Ke(5)*x(14)-
2*Vzeta(5)*x(7)*abs(x(7))-Kd(5)*t329*x(14)-Czeta(5)*x(7);;

% Calculate derivatives

        [m,n]=size(B);
        A1=B(:,1:n-1);
        f1=B(:,n);
        sys=zeros(1,2*m);
        sys(1:7)=A1\f1;
        sys(8:14)=x(1:7);

% Output states

elseif flag == 3

        sys(1:14)=x;

else

        sys = [];

end
```

APPENDIX C. H-3 PARAMETER VALUES

1. PARAMETER SETTING AND H-3 VALUE CHART

a. Roll Mode- 0% PWR Airborne

PARAMETER SETTINGS	H3 VALUE	UNITS
mb(1) mb(2) mb(3) mb(4) mb(5)	10	slugs
M(1) M(2)	504	slugs
R	8.75	feet
Omega	21.25	rad/sec
e1	1.05	feet
z	pi/12	radians
Phi(1) Phi(2) Phi(3) Phi(4) Phi(5)	0,2pi/5,4pi/5,6pi/5,8pi/5	radians
Czeta(1) Czeta(2) Czeta(3) Czeta(4) Czeta(5)	96320	ft-lbs/(rad/sec)
Vzeta(1) Vzeta(2) Vzeta(3) Vzeta(4) Vzeta(5)	0	ft-lbs/(rad/sec)^2
c(1) c(2)	254	lbs/(ft/sec)
v(1) v(2)	0	lbs/(ft/sec)^2
Ke(1) Ke(2) Ke(3) Ke(4) Ke(5)	0	ft-lbs/radian
Kd(1) Kd(2) Kd(3) Kd(4) Kd(5)	0	ft-lbs/radian^3
Ks(1) Ks(2) Ks(3) Ks(4) Ks(5)	0	ft-lbs/radian
K(1) K(2)	85690/2e7	lbs/ft
xXi xYi	xXi=0.2	ft
xrXi xrYi	0	ft/sec
x1i x2i x3i x4i x5i	0	radians
xr1i xr2i xr3i xr4i xr5i	0	radians/sec

b. Roll Mode-20% PWR Airborne

PARAMETER SETTINGS	H3 VALUE	UNITS
mb(1) mb(2) mb(3) mb(4) mb(5)	10	slugs
M(1) M(2)	504	slugs
R	8.75	feet
Omega	21.25	rad/sec
e1	1.05	feet
z	pi/12	radians
Phi(1) Phi(2) Phi(3) Phi(4) Phi(5)	0,2pi/5,4pi/5,6pi/5,8pi/5	radians
Czeta(1) Czeta(2) Czeta(3) Czeta(4) Czeta(5)	65189	ft-lbs/(rad/sec)
Vzeta(1) Vzeta(2) Vzeta(3) Vzeta(4) Vzeta(5)	0	ft-lbs/(rad/sec)^2
c(1) c(2)	410	lbs/(ft/sec)
v(1) v(2)	0	lbs/(ft/sec)^2

Ke(1) Ke(2) Ke(3) Ke(4) Ke(5)	0	ft-lbs/radian
Kd(1) Kd(2) Kd(3) Kd(4) Kd(5)	0	ft-lbs/radian^3
Ks(1) Ks(2) Ks(3) Ks(4) Ks(5)	0	ft-lbs/radian
K(1) K(2)	88653/2e7	lbs/ft
xXi xYi	xXi=0.2	ft
xrXi xrYi	0	ft/sec
x1i x2i x3i x4i x5i	0	radians
xr1i xr2i xr3i xr4i xr5i	0	radians/sec

c. Roll Mode-80% PWR Airborne

PARAMETER SETTINGS	H3 VALUE	UNITS
mb(1) mb(2) mb(3) mb(4) mb(5)	10	slugs
M(1) M(2)	504	slugs
R	8.75	feet
Omega	21.25	rad/sec
e1	1.05	feet
z	pi/12	radians
Phi(1) Phi(2) Phi(3) Phi(4) Phi(5)	0,2pi/5,4pi/5,6pi/5,8pi/5	radians
Czeta(1) Czeta(2) Czeta(3) Czeta(4) Czeta(5)	30452	ft-lbs/(rad/sec)
Vzeta(1) Vzeta(2) Vzeta(3) Vzeta(4) Vzeta(5)	0	ft-lbs/(rad/sec)^2
c(1) c(2)	1504	lbs/(ft/sec)
v(1) v(2)	0	lbs/(ft/sec)^2
Ke(1) Ke(2) Ke(3) Ke(4) Ke(5)	0	ft-lbs/radian
Kd(1) Kd(2) Kd(3) Kd(4) Kd(5)	0	ft-lbs/radian^3
Ks(1) Ks(2) Ks(3) Ks(4) Ks(5)	0	ft-lbs/radian
K(1) K(2)	131895/2e7	lbs/ft
xXi xYi	xXi=0.2	ft
xrXi xrYi	0	ft/sec
x1i x2i x3i x4i x5i	0	radians
xr1i xr2i xr3i xr4i xr5i	0	radians/sec

d. Lateral Mode-0% PWR Airborne

PARAMETER SETTINGS	H3 VALUE	UNITS
mb(1) mb(2) mb(3) mb(4) mb(5)	10	slugs
M(1) M(2)	215	slugs
R	8.75	feet
Omega	21.25	rad/sec
e1	1.05	feet
z	pi/12	radians

Phi(1) Phi(2) Phi(3) Phi(4) Phi(5)	0,2pi/5,4pi/5,6pi/5,8pi/5	radians
Czeta(1) Czeta(2) Czeta(3) Czeta(4) Czeta(5)	96320	ft-lbs/(rad/sec)
Vzeta(1) Vzeta(2) Vzeta(3) Vzeta(4) Vzeta(5)	0	ft-lbs/(rad/sec)^2
c(1) c(2)	80	lbs/(ft/sec)
v(1) v(2)	0	lbs/(ft/sec)^2
Ke(1) Ke(2) Ke(3) Ke(4) Ke(5)	0	ft-lbs/radian
Kd(1) Kd(2) Kd(3) Kd(4) Kd(5)	0	ft-lbs/radian^3
Ks(1) Ks(2) Ks(3) Ks(4) Ks(5)	0	ft-lbs/radian
K(1) K(2)	44544/2e7	lbs/ft
xXi xYi	xXi=0.2	ft
xrXi xrYi	0	ft/sec
x1i x2i x3i x4i x5i	0	radians
xr1i xr2i xr3i xr4i xr5i	0	radians/sec

e. Lateral Mode-20% PWR Mode

PARAMETER SETTINGS	H3 VALUE	UNITS
mb(1) mb(2) mb(3) mb(4) mb(5)	10	slugs
M(1) M(2)	215	slugs
R	8.75	feet
Omega	21.25	rad/sec
e1	1.05	feet
z	pi/12	radians
Phi(1) Phi(2) Phi(3) Phi(4) Phi(5)	0,2pi/5,4pi/5,6pi/5,8pi/5	radians
Czeta(1) Czeta(2) Czeta(3) Czeta(4) Czeta(5)	65189	ft-lbs/(rad/sec)
Vzeta(1) Vzeta(2) Vzeta(3) Vzeta(4) Vzeta(5)	0	ft-lbs/(rad/sec)^2
c(1) c(2)	106	lbs/(ft/sec)
v(1) v(2)	0	lbs/(ft/sec)^2
Ke(1) Ke(2) Ke(3) Ke(4) Ke(5)	0	ft-lbs/radian
Kd(1) Kd(2) Kd(3) Kd(4) Kd(5)	0	ft-lbs/radian^3
Ks(1) Ks(2) Ks(3) Ks(4) Ks(5)	0	ft-lbs/radian
K(1) K(2)	46471/2e7	lbs/ft
xXi xYi	xXi=0.2	ft
xrXi xrYi	0	ft/sec
x1i x2i x3i x4i x5i	0	radians
xr1i xr2i xr3i xr4i xr5i	0	radians/sec

71

f.   Lateral Mode-80% PWR Airborne

PARAMETER SETTINGS	H3 VALUE	UNITS
mb(1) mb(2) mb(3) mb(4) mb(5)	10	slugs
M(1) M(2)	215	slugs
R	8.75	feet
Omega	21.25	rad/sec
e1	1.05	feet
z	pi/12	radians
Phi(1) Phi(2) Phi(3) Phi(4) Phi(5)	0,2pi/5,4pi/5,6pi/5,8pi/5	radians
Czeta(1) Czeta(2) Czeta(3) Czeta(4) Czeta(5)	30452	ft-lbs/(rad/sec)
Vzeta(1) Vzeta(2) Vzeta(3) Vzeta(4) Vzeta(5)	0	ft-lbs/(rad/sec)^2
c(1) c(2)	350	lbs/(ft/sec)
v(1) v(2)	0	lbs/(ft/sec)^2
Ke(1) Ke(2) Ke(3) Ke(4) Ke(5)	0	ft-lbs/radian
Kd(1) Kd(2) Kd(3) Kd(4) Kd(5)	0	ft-lbs/radian^3
Ks(1) Ks(2) Ks(3) Ks(4) Ks(5)	0	ft-lbs/radian
K(1) K(2)	48152/2e7	lbs/ft
xXi xYi	xXi=0.2	ft
xrXi xrYi	0	ft/sec
x1i x2i x3i x4i x5i	0	radians
xr1i xr2i xr3i xr4i xr5i	0	radians/sec

g.   Coleman Test

For the remaining simulations, the only variance from the above parameters for each case was the change in Ω representing rotor speed and the zeroing out of pylon i.e. c(1) and rotor hub damping i.e. Czeta(1).

APPENDIX D. COLEMAN PLOTS

1.   COLEMAN.M

a.   No Damping Scenario-H-3

```
% nodamp1.m
% This program uses equation 31 introduced by Coleman and Feingold to
%represent how w and wf can be found specifically for the H-3.  This
%program plots only the real values of the answer for a no damping
%scenario.  The effect of lamda3 is shown in the plots.

close all
clear all

%real equation
lamda=0;
lamda1=0.05624;
lamda2=0;
lamda3=0;

K=1;      %stiffness s=1

wf=-5:.01:5;

wreal=(wf./(1-lamda1)).*(1+(lamda./(2*(-wf.^2+K))))+...
     (((wf./(1-lamda1)).*(1+(lamda./(2*(-wf.^2+K))))).^2+...
        (wf.^2./(1-lamda1)).*(-1+(lamda2./wf.^2)-
(lamda3.*wf.^2+lamda)./(-wf.^2+K))).^.5;

wreal1=(wf./(1-lamda1)).*(1+(lamda./(2*(-wf.^2+K))))-...
     (((wf./(1-lamda1)).*(1+(lamda./(2*(-wf.^2+K))))).^2+...
     (wf.^2./(1-lamda1)).*(-1+(lamda2./wf.^2)-(lamda3.*wf.^2+lamda)./(-
wf.^2+K))).^.5;

lamda3=0.022;

wreala=(wf./(1-lamda1)).*(1+(lamda./(2*(-wf.^2+K))))+...
     (((wf./(1-lamda1)).*(1+(lamda./(2*(-wf.^2+K))))).^2+...
        (wf.^2./(1-lamda1)).*(-1+(lamda2./wf.^2)-
(lamda3.*wf.^2+lamda)./(-wf.^2+K))).^.5;

wreal1a=(wf./(1-lamda1)).*(1+(lamda./(2*(-wf.^2+K))))-...
     (((wf./(1-lamda1)).*(1+(lamda./(2*(-wf.^2+K))))).^2+...
     (wf.^2./(1-lamda1)).*(-1+(lamda2./wf.^2)-(lamda3.*wf.^2+lamda)./(-
wf.^2+K))).^.5;

lamda3=0.44;

wrealb=(wf./(1-lamda1)).*(1+(lamda./(2*(-wf.^2+K))))+...
     (((wf./(1-lamda1)).*(1+(lamda./(2*(-wf.^2+K))))).^2+...
```

73

```
        (wf.^2./(1-lamda1)).*(-1+(lamda2./wf.^2)-
(lamda3.*wf.^2+lamda)./(-wf.^2+K))).^.5;

wreal1b=(wf./(1-lamda1)).*(1+(lamda./(2*(-wf.^2+K))))-...
    (((wf./(1-lamda1)).*(1+(lamda./(2*(-wf.^2+K)))))).^2+...
    (wf.^2./(1-lamda1)).*(-1+(lamda2./wf.^2)-(lamda3.*wf.^2+lamda)./(-
wf.^2+K))).^.5;

hold on
plot(wreal,wf,'b--',wreal1,wf,'b--',wreala,wf,'r-.',wreal1a,wf,'r-
.',wrealb,wf,'r',wreal1b,wf,'r')    %like a charm I-8
hold off
axis([-1 4 -1 3])
grid
ylabel('wf')
xlabel('w')
title('Effect of coupling between pylon and hinge motions-H-3-no
damping')
%legend('lamda3=0','lamda3=0.2','lamda3=0.4')
gtext('lamda3=0')
gtext('0.2')
gtext('0.4')
%gtext('stable region')
%gtext('unstable region')
gtext('A')
gtext('B')
gtext('C')
gtext('zero coupling')
%gtext('hinge deflection')
%gtext('pylon bending')
```

b.   Damping Scenario-H-3

```
% damp1.m
% The following program uses Coleman's equation(31)to calculate w and
%wf for a damped case specific to H-3.
close all
clear all

%real equation
lamdap=.059;
lamdaphi=1.19;
lamda=lamdap*lamdaphi;
lamda1=0.05624;
lamda2=0;
lamda3=0.044226;
K=1;      %stiffness s=1

wf=-5:.01:5;

wreal=(wf./(1-lamda1)).*(1+(lamda./(2*(-wf.^2+K))))+...
```

74

```
     (((wf./(1-lamda1)).*(1+(lamda./(2*(-wf.^2+K)))))).^2+...
        (wf.^2./(1-lamda1)).*(-1+(lamda2./wf.^2)-
(lamda3.*wf.^2+lamda)./(-wf.^2+K))).^.5;

wreal1=(wf./(1-lamda1)).*(1+(lamda./(2*(-wf.^2+K))))-...
     (((wf./(1-lamda1)).*(1+(lamda./(2*(-wf.^2+K)))))).^2+...
     (wf.^2./(1-lamda1)).*(-1+(lamda2./wf.^2)-(lamda3.*wf.^2+lamda)./(-
wf.^2+K))).^.5;


   %imaginary equation

 wimag=(1/(1-lamda1)).*(wf-(lamdaphi./(2.*lamdap.*wf)).*(-wf.^2+K))+...
 sqrt(((1/(1-lamda1)).*(wf-(lamdaphi./(2.*lamdap.*wf)).*(-
wf.^2+K))).^2+...
        (1/(1-lamda1)).*((lamdaphi/lamdap).*(-wf.^2+K)+(-
wf.^2+lamda2)));

 wimag1=(1/(1-lamda1)).*(wf-(lamdaphi./(2.*lamdap.*wf)).*(-wf.^2+K))-
...
   sqrt(((1/(1-lamda1)).*(wf-(lamdaphi./(2.*lamdap.*wf)).*(-
wf.^2+K))).^2+...
        (1/(1-lamda1)).*((lamdaphi/lamdap).*(-wf.^2+K)+(-
wf.^2+lamda2)));

%gtext('stable region')
%gtext('stable region')
%gtext('unstable region')
%gtext('hinge deflection')
%gtext('pylon bending')

hold on
figure(1)
plot(wreal,wf,'r',wreal1,wf,'r')
plot(wimag,wf,'b--',wimag1,wf,'b--')
hold off
axis([-1 4 -1 3])
grid
ylabel('wf')
xlabel('w')
title('Plot of real and imaginary cases for the H-3')
legend('r','real','b--','imaginary')
%gtext('A')
gtext('B')
%gtext('C')
```

INITIAL DISTRIBUTION LIST

1. Defense Technical Information Center 2
   8725 John J. Kingman Rd., Suite 0944
   Ft. Belvoir, VA 22060-6218

2. Dudley Knox Library 2
   Naval Postgraduate School
   411 Dyer Rd.
   Monterey, CA 93943-5101

3. Chairman, Code AA/Co 1
   Department of Aeronautics and Astronautics
   Naval Postgraduate School
   Monterey, CA 93943-5000

4. Prof. E. Roberts Wood, Code AA/Wd 2
   Department of Aeronautics and Astronautics
   Naval Postgraduate School
   Monterey, CA 93943-5000

5. LCDR Robert L. King USN, Code AA/Ki 1
   Department of Aeronautics and Astronautics
   Naval Postgraduate School
   Monterey, CA 93943-5000

6. Dr. Robert Ormiston 1
   U. S. Army Aeroflightdynamics Dir.
   NASA Ames Research Center
   Moffet Field, CA 94035

7. Louis J. Silverthorn 1
   Boeing Helicopters-Mesa
   5000 E. McDowell Rd 510/A387
   Mesa, AZ 85215

8. Mr. W. Euan Hooper 1
   729 Rhoads Dr.
   Springfield, PA 19064-1609

9. Mr. Jerry March 1
   Advanced Office Systems INC.
   P.O. Box 990
   Los Gatos, CA 95031